BUREAU OF RECLAMATION

Final Report No. ST-2023-21041

# Combining Physically Based Snow Modeling and Remote Sensing at High Spatial Resolution to Improve Snowmelt Runoff Forecasts in the Big Thompson and Willow Creek Basins

**Research and Development Office**

**Science and Technology**

Research Program

U.S. Department of the Interior

October 2025

# REPORT DOCUMENTATION PAGE

*Form Approved*
*OMB No. 0704-0188*

The public reporting burden for this collection of information is estimated to average 1 hour per response, including the time for reviewing instructions, searching existing data sources, gathering and maintaining the data needed, and completing and reviewing the collection of information. Send comments regarding this burden estimate or any other aspect of this collection of information, including suggestions for reducing the burden, to Department of Defense, Washington Headquarters Services, Directorate for Information Operations and Reports (0704-0188), 1215 Jefferson Davis Highway, Suite 1204, Arlington, VA 22202-4302. Respondents should be aware that notwithstanding any other provision of law, no person shall be subject to any penalty for failing to comply with a collection of information if it does not display a currently valid OMB control number.
PLEASE DO NOT RETURN YOUR FORM TO THE ABOVE ADDRESS.

| 1. REPORT DATE (DD-MM-YYYY) | 2. REPORT TYPE | 3. DATES COVERED *(From - To)* |
|---|---|---|
| September 30, 2025 | Research | October 2020 – September 2023 |

| 4. TITLE AND SUBTITLE | |
|---|---|
| Combining Physically Based Snow Modeling and Remote Sensing at High Spatial Resolution to Improve Snowmelt Runoff Forecasts in the Big Thompson and Willow Creek Basins | 5a. CONTRACT NUMBER<br>RY.15412021.WP21041 |
| | 5b. GRANT NUMBER |
| | 5c. PROGRAM ELEMENT NUMBER<br>1541 (S&T) |
| 6. AUTHOR(S)<br>Claudia Leon-Salazar, PhD (Reclamation)<br>Graham Sexstone, PhD (USGS)<br>David Selkowitz, PhD (USGS)<br>Garrett, Akie (USGS)<br>Emily Carbone (Northern Water)<br>Lindsay Bearup, PhD (Reclamation) | 5d. PROJECT ID NUMBER<br>Final Report ST-2025-21041 |
| | 5e. TASK NUMBER |
| | 5f. WORK UNIT NUMBER |

| 7. PERFORMING ORGANIZATION NAME(S) AND ADDRESS(ES) | | 8. PERFORMING ORGANIZATION REPORT NUMBER |
|---|---|---|
| United States Department of Interior<br>Bureau of Reclamation<br>Eastern Colorado Area Office<br>11056 West County Road 18E<br>Loveland, CO 80537 | United States Department of Interior<br>US Geological Survey<br>Denver Federal Center<br>PO Box 25046, MS 415<br>Denver, CO 80225 | Eastern Colorado Area Office |
| 9. SPONSORING/MONITORING AGENCY NAME(S) AND ADDRESS(ES)<br>Science and Technology Program<br>Research and Development Office<br>Bureau of Reclamation<br>U.S. Department of the Interior<br>Denver Federal Center<br>PO Box 25007, Denver, CO 80225-0007 | | 10. SPONSOR/MONITOR'S ACRONYM(S)<br>Reclamation |
| | | 11. SPONSOR/MONITOR'S REPORT NUMBER(S) (if applicable)<br>Final Report ST-2023-21041 |

12. DISTRIBUTION/AVAILABILITY STATEMENT
Final Report may be downloaded from https://www.usbr.gov/research/projects/index.html

13. SUPPLEMENTARY NOTES

14. ABSTRACT

In basins dominated by snowmelt during the spring and early summer, runoff forecast methods often rely on snowpack information from spatial products with coarse resolution (1 km) and/or in-situ observations across limited geographic locations both of which are not always representative of basin snow conditions. Accurate characterization of snow water equivalent (SWE) requires representing its spatial variability across the basin scale with sufficiently fine spatial resolution to account for important processes that drive seasonal snowpack evolution. This study developed 30-m SnowModel simulations across the Big Thompson River, Three Lakes, and Willow Creek Basins, Colorado (4,212 km$^2$) for water years 2000 through 2023 and evaluated the incorporation of remotely sensed snow-covered area (SCA) datasets into model development and calibration. Results show that versions of SnowModel calibrated to remotely sensed SCA had improved performance over baseline simulations especially at the highest elevations. This study also developed a near real-time modeling approach that couples remotely sensed SCA data at 30-m resolution with the calibrated SnowModel simulations to further improve the spatial distribution of simulated snow across the study basins. Results from this near real time tool are currently being used by Eastern Colorado Area Office (ECAO) to inform ECAO's streamflow forecasting system.

15. SUBJECT TERMS
Satellite Remote Sensing, Snow Cover, Snow Modeling, Snow Water Equivalent, Streamflow Forecasting

| 16. SECURITY CLASSIFICATION OF: | | | 17. LIMITATION OF ABSTRACT | 18. NUMBER OF PAGES | 19a. NAME OF RESPONSIBLE PERSON |
|---|---|---|---|---|---|
| | | | | 65 | Claudia Leon-Salazar |
| a. REPORT | b. ABSTRACT | c. THIS PAGE | | | 19b. TELEPHONE NUMBER *(Include area code)* |
| U | U | U | | | 970-461-5462 |

**Standard Form 298** (Rev. 8/98)
Prescribed by ANSI Std. Z39.18

# Mission Statements

The U.S. Department of the Interior protects and manages the Nation's natural resources and cultural heritage; provides scientific and other information about those resources; honors its trust responsibilities or special commitments to American Indians, Alaska Natives, Native Hawaiians, and affiliated Island Communities.

The mission of the Bureau of Reclamation is to manage, develop, and protect water and related resources in an environmentally and economically sound manner in the interest of the American public.

# Disclaimer

Information in this report may not be used for advertising or promotional purchases. The data and findings should not be construed as an endorsement of any product or firm by the Bureau of Reclamation, Department of Interior, or Federal Government. The products evaluated in the report were evaluated for purposes specific to the Bureau of Reclamation mission. Reclamation gives no warranties or guarantees, expressed or implied, for the products evaluated in this report, including merchantability or fitness for a particular purpose.

# Acknowledgements

The Science and Technology Program, Bureau of Reclamation, sponsored this research. Additional funding was provided by Northern Colorado Water Conservancy District and by the U.S. Geological Survey.

**Cover Image** – Picture of Loch Vale in Rocky Mountain National Park 2023 winter season. It shows snow along the alpine area and rocky peaks (U.S. Geological Survey).

# Combining Physically Based Snow Modeling and Remote Sensing at High Spatial Resolution to Improve Snowmelt Runoff Forecasts in the Big Thompson and Willow Creek Basins

**Final Report No. ST-2025-21041**


Prepared by:

**Reclamation Eastern Colorado Area Office**
**Claudia Leon-Salazar, PhD, Civil Engineer (Hydrologic)**

**U.S. Geological Survey**
**Graham Sexstone, PhD, Research Hydrologist**
**David Selkowitz, PhD, Research Geographer**
**Garrett Akie, Hydrologist**

**Northern Colorado Water Conservancy District**
**Emily Carbone, Water Resources Specialist**

**Reclamation Technical Service Center**
**Lindsay Bearup, PhD, Civil Engineer**

# Peer Review

## Bureau of Reclamation
## Research and Development Office
## Science and Technology
## Research Program

**Final Report ST-2025-21041**

**Combining Physically Based Snow Modeling and Remote Sensing at High Spatial Resolution to Improve Snowmelt Runoff Forecasts in the Big Thompson and Willow Creek Basins**

CLAUDIA LEON SALAZAR Digitally signed by CLAUDIA LEON SALAZAR
Date: 2026.01.30 12:57:01 -07'00'

Prepared by: Claudia A. Leon-Salazar, PhD
Civil Engineer (Hydrologic), Bureau of Reclamation

JAMES VANSHAAR Digitally signed by JAMES VANSHAAR
Date: 2026.01.30 15:41:39 -07'00'

Supervisor: James VanShaar, PE
Supervisory Civil Engineer (Hydrologic), Bureau of Reclamation

This document has been reviewed under the Research and Development Office Discretionary peer review process, consistent with Reclamation Policy CMP P14. It does not represent and should not be construed to represent the Bureau of Reclamation's determination, concurrence, or policy.

# Acronyms and Abbreviations

| | |
|---|---|
| ASO | Airborne Snow Observatories |
| C-BT | Colorado Colorado-Big Thompson Project |
| ECAO | Eastern Colorado Area Office |
| HLS | Harmonized Landsat Sentinel |
| $km^2$ | square kilometer(s) |
| m | meter(s) |
| $mi^2$ | square mile(s) |
| mm | millimeters |
| MODIS | Moderate Resolution Imaging Spectroradiometer |
| NRCS | Natural Resource Conservation Service |
| NLDAS-2 | Phase 2 North American Land Data Assimilation System |
| Northern | Northern Colorado Water Conservancy District |
| Reclamation | Bureau of Reclamation |
| SCA | Snow Covered Area |
| SNODAS | Snow Data Assimilation System |
| SNOTEL | SNOwpack TELemetry Network |
| SWE | Snow Water Equivalent |
| USGS | U.S. Geological Survey |

## Symbols

| | |
|---|---|
| > | greater than |
| < | less than |
| × | multiplied by |
| % | percent |

# Contents

Page

Executive Summary ..... ES-1
1.0 Introduction ..... 1
2.0 Data ..... 1
2.1. SnowModel input and output files ..... 1
3.0 References ..... 3

## Appendices

A Peer-Reviewed Article: Fine-Resolution Satellite Remote Sensing Improves Spatially Distributed Snow Modeling to Near Real Time

# Executive Summary

Bureau of Reclamation Eastern Colorado Area Office (ECAO) and Northern Water Conservancy District (Northern) are responsible for the maintenance and operation of the Colorado-Big Thompson Project (C-BT) in Northern Colorado. The C-BT imports water from the Collection System in the headwaters of the Colorado River to the Front Range on the east slope of the Continental Divide, where import water mixes with runoff from the Big Thompson River basin at Lake Estes. The study area includes the basins draining into the Collection System and to Lake Estes.

As managers of the C-BT, ECAO and Northern forecast inflow to the system reservoirs. Runoff from the C-BT basins is typically dominated by snowmelt during the spring and early summer months. Existing runoff forecast methods rely mostly on modeled daily estimates of snow water equivalent (SWE) across the basins at coarse spatial resolution (1 km) such as Snow Data Assimilation System (SNODAS) and in-situ observations at limited locations below the treeline. These data sources underestimate SWE particularly in late spring and early summer months when the remaining snowpack in the basins is distributed across a matrix of deep snow patches interspersed with snow-free ground across the high elevation alpine zone. This deficiency in the data limits the accuracy of runoff forecasts.

Given the highly variable distribution of the seasonal snowpack in these complex mountainous environments, accurate modeling of basin-wide SWE requires a spatially distributed approach at a sufficiently fine grid resolution to account for important processes in the seasonal evolution of the snowpack (e.g., wind redistribution of snow to resolve patchy snow cover in the alpine zone). However, even state-of-the art, well-validated snow evolution models are prone to errors when key model inputs such as precipitation and wind speed/direction are inaccurate or only available at very coarse spatial resolutions. Incorporating regularly updated high spatial resolution remotely sensed Snow-Covered Area (SCA) can substantially reduce model errors resulting from coarse resolution or inaccurate precipitation and wind input data. An alternative approach is to use Airborne Snow Observatories (ASO) SWE products (Painter et al. 2016). ASO SWE can capture high elevation snow accurately, but requires a separate lidar flyover for each measurement, incurring significant cost.

ECAO and Northern partnered with the U.S. Geological Survey (USGS) for this study to develop a near real-time modeling approach that provides a more accurate representation and estimates of SWE for the study area. The modeling approach couples two major sub-systems: 1) a remote sensing tool that provides near real-time SCA data at 30-m resolution and, 2) a physically based and spatially distributed snow evolution model that simulates snow processes relevant in the study basins such as wind redistribution and canopy interception to produce basin wide SWE estimates. The remote sensing tool provides SCA to the snow modeling tool to further improve the spatial distribution of simulated snow across the basins.

The near real-time remote sensing tool relies on low latency surface reflectance datasets to produce SCA. The tool uses NASA's Harmonized Landsat Sentinel (HLS) surface reflectance data, which combines Landsat and Sentinel 2 data streams. A machine learning approach was used to produce near real-time SCA using HLS as input data. This approach is in good

agreement with the spectral unmixing approach currently used for USGS Landsat Level 3 Fractional SCA product. The new approach works equally well for Landsat and Sentinel 2 datasets and can be used to generate SCA updates as soon as the HLS surface reflectance product for each new acquisition becomes available, typically within 48 hours of satellite overpass. Another important output from the remote sensing analysis was the generation of a mean annual snow cover persistence map from historical Landsat images spanning from 1984 to present. This map provides a detailed and accurate representation of long-term snow cover patterns used to guide the snow model calibration.

The snow modeling tool, SnowModel (Liston and Elder 2006), was implemented for an area of 4,212 square kilometer ($km^2$) (1,626 square miles [$mi^2$]) with a grid cell size of 30 meters (m). The model was calibrated using historical meteorological forcings from the Phase 2 North American Land Data Assimilation System (NLDAS-2) from water years 2000 to 2020. A range of SnowModel parameters that define snow density evolution, wind redistribution of snow, and snow albedo were calibrated using a Latin Hypercube sampling in a stepwise process (Akie et. al 2024). The spatial distribution of snow was calibrated to the Landsat long-term snow cover persistence and the temporal variability of snow was calibrated to Moderate Resolution Imaging Spectroradiometer (MODIS) snow-covered area. As part of the calibration effort, a precipitation correction factor grid was developed to adjust the calibrated model for biases in the meteorological data. This precipitation correction grid was developed according to relationships among the mean annual snow persistence map, the snow persistence and peak SWE at SNOwpack TELemetry Network (SNOTEL) stations and the calibrated SnowModel outputs. SnowModel calibration results were evaluated against ASO data collected in April and May 2022 in the Windy Gap and Big Thompson River basins. The calibration results are in good agreement with the ASO SWE spatial patterns. However, SnowModel SWE tends to be lower than ASO SWE at low and high elevation bands. To further improve the SnowModel results in the real time environment, the SnowModel was configured to assimilate the pseudo real-time HLS SCA data.

ECAO tested SWE results from the pseudo real-time system for the Big Thompson River basin during the 2023 runoff season. Unadjusted and adjusted SnowModel results agreed with SNODAS SWE in the upper elevation band of the basin (above 10,250 ft) from about March to mid-June. After mid-June, the unadjusted SnowModel results showed that the snow in the basin was completely depleted which also agreed with the SNODAS dataset. However, the results of the adjusted SnowModel with remotely sensed data showed a significant amount of remaining snow in the upper elevation band. ECAO used the adjusted SnowModel SWE time series to guide the model states within its existing hourly runoff forecasting system. This adjustment in the hourly runoff forecasting system improved the short-term streamflow prediction above Lake Estes. Another important outcome of this project is the generation of historical SWE time series from the SnowModel calibration. ECAO is planning to incorporate these time series within existing statistical regression models to generate water supply forecasts and evaluate the potential improvements in forecast.

# 1.0 Introduction

The Introduction, Methodology, pertinent data, and results for this project are included in the journal article attached in appendix A of this report.

The article is also available in the following link:
https://www.mdpi.com/2072-4292/17/10/1704

This is the citation for the article:

Sexstone, G.A.; Akie, G.A.; Selkowitz, D.J.; Barnhart, T.B.; Rey, D.M.; León-Salazar, C.; Carbone, E.; Bearup, L.A. Fine-Resolution Satellite Remote Sensing Improves Spatially Distributed Snow Modeling to Near Real Time. Remote Sens. 2025, 17, 1704. https://doi.org/10.3390/ rs17101704

# 2.0 Data

## 2.1. SnowModel input and output files

SnowModel input and output files generated for this project are stored in the following USGS data release:

Akie, G.A., Barnhart, T.B., Selkowitz, D.J., and Sexstone, G.A., 2025, Historical simulated snowpack for the Willow Creek and Big Thompson, Colorado watersheds and vicinity, water years 1994–2023: U.S. Geological Survey data release, https://doi.org/10.5066/P9NTGM51.

**Point of Contact name, email, and phone:** Garrett Akie, gakie@usgs.gov, 303-236-6923
**Short description of the data:** All data stored in USGS data release (see citation above) consists of model code and input text configuration files to reproduce SnowModel simulations and NetCDF SnowModel output files including snow water equivalent (SWE) as well as other model variables.

**Keywords:** Snowpack, SWE, Snow modeling, Water supply forecasting
**Approximate total size of all files:** (folder size) approximately 2 TB

# 3.0 References

Akie, G.A., T.B. Barnhart, D.J. Selkowitz, and G.A. Sexstone. (2024). Historical simulated snowpack for the Willow Creek and Big Thompson, CO watersheds and vicinity, water years 1994–2023: U.S. Geological Survey Data Release, https://doi.org/10.5066/P9NTGM51.

Liston, G. E., and K. Elder. 2006. A Distributed Snow-Evolution Modeling System (SnowModel). *Journal of Hydrometeorology* 7(6): 1259–1276. https://doi.org/10.1175/JHM548.1.

Painter, T.H., D.F. Berisford, J.W. Boardman, et al. 2016. The Airborne Snow Observatory: Fusion of scanning lidar, imaging spectrometer, and physically-based modeling for mapping snow water equivalent and snow albedo. *Remote Sensing of Environment* 184: 139–152.

# Appendix A

Peer-Reviewed Article: Fine-Resolution Satellite Remote Sensing Improves Spatially Distributed Snow Modeling to Near Real Time

# Fine Resolution Satellite Remote Sensing Improves Near Real-Time Spatially Distributed Snow Modeling

**Graham A. Sexstone [1,*], Garrett A. Akie [1], David J. Selkowitz [2], Theodore B. Barnhart [2], David M. Rey [3], Claudia León-Salazar [4], Emily Carbone [5], and Lindsay A. Bearup [6]**

[1] U.S. Geological Survey, Colorado Water Science Center, Lakewood, CO, USA
[2] U.S. Geological Survey, Wyoming-Montana Water Science Center, Helena, MT, USA
[3] U.S. Geological Survey, Water Mission Area–Observing Systems Division, Hydrologic Remote Sensing Branch, Lakewood, CO, USA
[4] U.S. Bureau of Reclamation, Eastern Colorado Area Office, Loveland, CO, USA
[5] Northern Colorado Water Conservancy District, Berthoud, CO, USA
[6] U.S. Bureau of Reclamation, Technical Service Center, Lakewood, CO, USA

Abstract: Given the highly variable distribution of seasonal snowpacks in complex mountainous environments, accurate snow modeling of basin-wide snow water equivalent (SWE) requires a spatially distributed approach at a sufficiently fine grid resolution (< 500 meters) to account for important processes in the seasonal evolution of the snowpack (e.g., wind redistribution of snow to resolve patchy snow cover in the alpine zone). However, even well-validated snow evolution models, such as SnowModel, are prone to errors when key model inputs, such as precipitation and wind speed and direction, are inaccurate or only available at coarse spatial resolutions. Incorporating fine spatial resolution remotely sensed snow-covered area (SCA) information into spatially distributed snow modeling has the potential to refine and improve fine resolution snow water equivalent (SWE) estimates. This study developed 30-meter resolution SnowModel simulations across the Big Thompson River, Fraser River, Three Lakes, and Willow Creek Basins, a total area of 4,212 $km^2$, in Colorado for water years 2000–2023 and evaluated the incorporation of Moderate Resolution Imaging Spectroradiometer (MODIS) and Landsat SCA datasets into model development and calibration. SnowModel was calibrated spatially to Landsat mean annual snow persistence (SP) and temporally to MODIS mean basin SCA using a multi-objective calibration procedure explored through Latin hypercube sampling and a stepwise calibration process. Landsat mean annual SP was also used to further optimize SnowModel simulations through the development of a spatially variable precipitation correction field. Evaluations of SnowModel simulations using light detection and ranging (lidar)-derived Airborne Snow Observatories (ASO) SWE estimates show that versions of SnowModel calibrated to remotely sensed SCA had improved performance (mean error ranging from -28 mm to -6 mm) compared with baseline simulations (mean error ranging from 69 millimeters (mm) to 86 mm) and comparable spatial patterns to ASO especially at the highest elevations. Furthermore, study results highlight how regularly updated 30-meter resolution SCA could be used to further improve the calibrated SnowModel simulations in near real-time (latency of 5 days or less).

**Keywords**: snow; hydrology; remote sensing; snow covered area; snow persistence; SnowModel; Landsat; real time; streamflow forecasting; spatially distributed snow modeling

# A-1. Introduction

Across the western United States, 71 percent (%) of the annual streamflow has been estimated to originate as snowmelt [1]. In the semi-arid, high-elevation headwaters of the over allocated Upper Colorado River Basin, an even greater fraction of streamflow is generated by snowmelt (>80%), and year-to-year streamflow variability is driven by the seasonal accumulation of snowpack water storage and its subsequent melting [2]. Seasonal mountain snowpacks function as large natural reservoirs, accumulating water during winter and spring each year and releasing it through snowmelt during spring and summer when water demands are greatest [3]. Optimal management of water in the western United States requires an accurate streamflow forecasting skill that depends heavily on mountain snowpack information [4–6]. Thus, the near real-time (defined in this study as having a latency of 5 days or less) characterization of seasonal snow resources and the timing and magnitude of their release are vital and timely for supporting water resources management and decision making [7–10].

An inadequate characterization of the snowpack is a major source of error for streamflow forecasts. This is especially true for years with anomalous patterns of snow accumulation and melt, which are occurring more frequently because of changing climate [2]. A challenge in characterizing seasonal snow is that it exhibits complex spatial and temporal variability across the landscape [11, 12]. Meteorological drivers and their interactions with topography and land surface features, such as forests, strongly influence snowpack evolution and snow variability through snow accumulation, wind redistribution, sublimation, and snowmelt processes [13–15]. The Natural Resource Conservation Service (NRCS) operates the SNOwpack TELemetry Network (SNOTEL), providing critically important in-situ snow water equivalent (SWE) observations across the western United States [16]. However, in the Upper Colorado River Basin, seasonal snowpacks cover a large range in elevation that contains a substantial alpine area above treeline, and current snowpack monitoring stations do not fully represent this range of land covers, elevations, and terrain classes [8, 17]. Furthermore, snow measured at monitoring stations may not adequately represent snow patterns within surrounding areas [18–20]. Given the highly variable distribution of the seasonal snowpack in complex mountainous environments, accurate quantification of basinwide SWE evolution requires a spatially distributed approach at a sufficiently fine grid resolution to account for important processes in the seasonal evolution of the snowpack (e.g., wind redistribution of snow to resolve patchy snow cover in the alpine zone). Many studies have developed retrospective snow modeling techniques and datasets that leverage remotely sensed snow-covered area (SCA) observations during the snow depletion season to reconstruct spatially distributed SWE information [20–22].

Spatiotemporal snow estimation techniques developed by recent studies that combine remotely sensed data, spatial modeling and reanalysis, and ground-based observations in data-model fusion approaches [e.g., 23, 24] have shown promise for assessments of near real-time snow water storage within seasonally snow-covered catchments. Although retrospective modeling approaches cannot be applied in near real time, recent studies have combined these retrospective datasets with additional statistical techniques to develop real-time SWE estimation techniques

with considerable success [24–26]. A challenge of these statistically based modeling approaches is that they rely heavily on ground SWE observations, which are not always available or can be situated in locations that do not hold snow late in the ablation season.

Operationally, the National Weather Service provides near real-time daily 1 kilometer (km) resolution gridded estimates of SWE for the conterminous US through the Snow Data Assimilation (SNODAS) program that combines spatially distributed snow modeling and data assimilation of ground- and remote sensing-based snow observations [27]. SNODAS data provide an important and widely available spatiotemporal SWE data source that can be used to support water resources forecasting. However, these relatively coarse spatial resolution model estimates have been shown to underestimate SWE in the late spring and early summer months when the remaining snowpack is distributed across a matrix of deep snow patches interspersed with snow-free ground across the high elevation alpine zone [28–30].

Additionally, many studies have focused on combining process-based snow modeling with the assimilation of optical satellite remote sensing of snow-cover information [31]. Most of these studies have utilized moderate resolution satellite (e.g., Moderate Resolution Imaging Spectroradiometer [MODIS]) SCA observations [e.g., 32–35], whereas few studies have evaluated the utility of using fine resolution satellite (e.g., Landsat, Sentinel-2) SCA observations [36,37]. A substantial challenge of process-based snow modeling approaches arises from uncertainties associated with atmospheric forcing data [38]. However, data assimilation approaches [31] can be used to reduce these uncertainties, and process-based modeling approaches can be operated in near real-time anywhere on earth where snow occurs.

Lastly, aircraft-based light detection and ranging (lidar) can be used to measure snow-on and snow-off elevation surfaces to derive highly accurate snow depth distributions at very fine spatial resolutions [39]. Airborne Snow Observatories (ASO) combines snow density estimates from process-based snow modeling constrained by ground observations with lidar-derived snow depths to provide near real-time SWE estimates at a 50 meter (m) spatial resolution across the basin scale [40, 41]. Although ASO datasets are only available for snapshots in both space and time, these highly accurate datasets are being used to support water resources forecasting and are increasingly being considered as ground “truth” for the evaluation of other SWE products [e.g., 42].

The objective of this study is to evaluate how fine spatial resolution remotely sensed SCA information has the potential to improve near real-time SWE estimates developed through spatially distributed process-based snow modeling. We leverage recently collected independent ASO datasets to evaluate snow modeling calibrated and constrained by 30-m spatial resolution remotely sensed snow-cover information. To address our study objective, we ask (1) How can a physically based snow model be calibrated using historical remotely sensed snow cover? (2) What improvements are made when utilizing historical remotely sensed snow cover compared to baseline snow modeling techniques? And (3) Can real-time post-processing of snow modeling output based on observed snow cover further improve model accuracy?

# A-2. Materials and Methods

## A-2.1 Study Area

The study area was a 78 km × 54 km (4,212 $km^2$) model domain in the north-central Colorado Rocky Mountains, US, ranging in elevation from 2,278 meters (m) to 4,345 m above sea level (figure A-1). The study area encompassed the headwaters of the Upper Colorado, North Platte, and South Platte River Basins. The land cover of the study area was composed of approximately 17% bare rock and alpine tundra area above treeline, 66% forested area, and 17% non-forested areas below treeline [43]. The East Troublesome Fire was a large wildfire (784 km2) that occurred within parts of the study area between October and November 2020 [figure A-1; 44]. The study area is positioned within a snow-dominated mountainous region that accumulates deep seasonal snowpacks, and the year-to-year variability in streamflow is mainly driven by snowpack water storage and subsequent snowmelt [2].

## A-2.2 Model Description and Simulations

To simulate detailed snow evolution processes across the study area, we utilized SnowModel, a spatially distributed, time-evolving, physically based snow modeling system designed for application in a wide range of environments where snow occurs [figure A-2; 47–49]. SnowModel includes the following submodels: MicroMet [50], a high-resolution meteorological distribution model; EnBal [51], a model of surface energy exchange between the snow and atmosphere; SnowPack [52], a seasonal evolution model of snow depth, snow density, and SWE; SnowTran-3D [53, 54], a three dimensional model of snow redistribution by wind across topographically variable terrain; and SnowAssim [55], a data assimilation system used for assimilating observations into SnowModel. SnowModel includes the physics required to simulate all first-order processes governing the seasonal evolution of the snowpack including blowing-snow redistribution and snow sublimation [15, 48]. SnowModel has been shown to perform well in seasonally snow-covered environments within and similar to the study area [e.g., 8, 15, 30, 56–58].

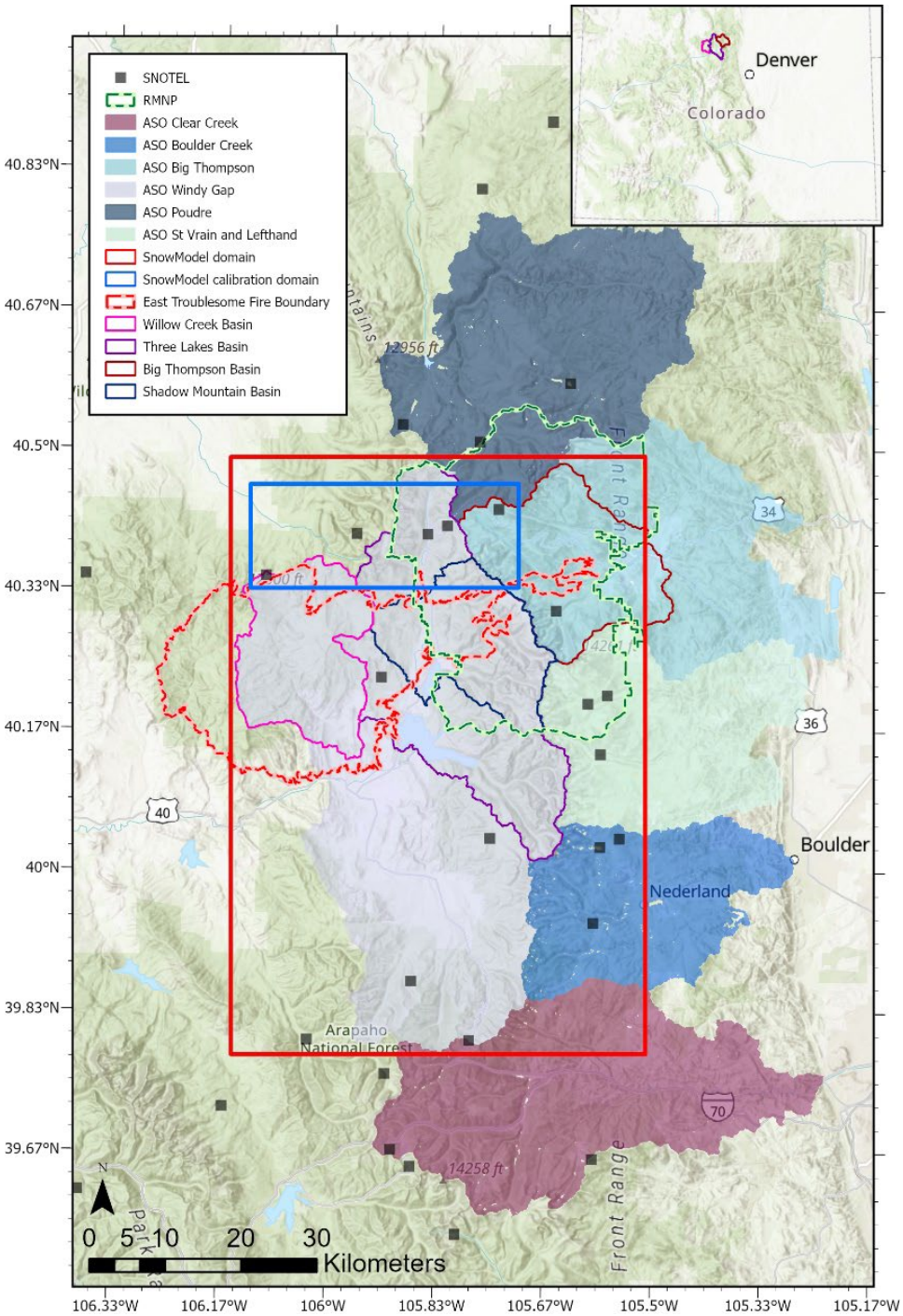


**Figure A-1.—Study area map showing the (1) snow modeling domain location within the north-central Colorado Rocky Mountains, US [43], (2) snow modeling calibration domain within the study area [43], (3) boundary of Rocky Mountain National Park (RMNP), (4) boundary of the East Troublesome Fire [44], (5) basin areas of interest within the study area, (6) SNOwpack TELemetry Network (SNOTEL) station locations [45], and (7) Airborne Snow Observatories (ASO) survey areas [46].**

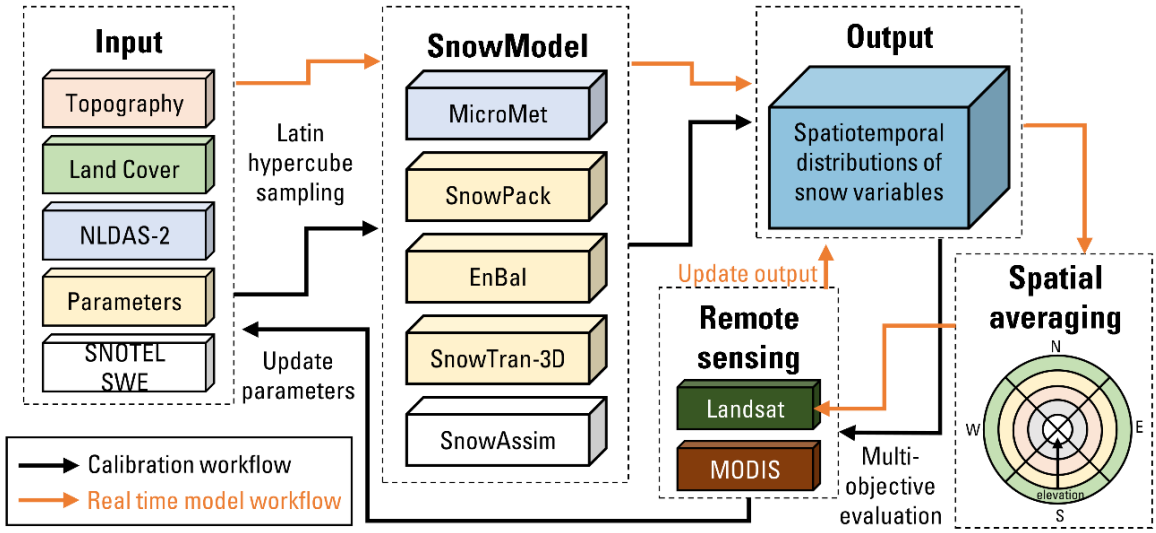


**Figure A-2.—Conceptual diagram of SnowModel inputs, submodels, and outputs along with a flow chart of the workflows used in this study for calibration and real-time application and post processing. Diagram modified from previous publication [59].**

SnowModel simulations were run at a 3-hour time step with a 30-m spatial grid resolution for water years (from 1 October to 31 September) 2000 through 2023. Elevation, canopy cover fraction, and land cover for the model domain were provided by the U.S. Geological Survey (USGS) National Elevation Dataset [60], USGS National Land Cover Database [61], and the National Park Service (NPS) Vegetation Mapping Inventory Project for Rocky Mountain National Park [62; Supporting Information S1], respectively. Effective leaf area index (LAI*) values across the domain were generated by scaling the maximum LAI* for each forest class vegetation type by the canopy cover fraction [e.g., 15, 58]. The LAI* for burned forest areas were adjusted based on the methods described in Sexstone et al. [58]. Furthermore, this study uses the snow albedo decay parameterization to represent snow albedo decay in non-forested, forested, and burned forest areas for both non-melting and melting snow conditions presented by Sexstone et al. [58]. Meteorological forcing data for the SnowModel simulations were provided by the 1/16° grid spacing near real-time North American Land Data Assimilation System (NLDAS-2) reanalysis forcing dataset [63]. NLDAS-2 was used for this study as it provides (1) the sub-daily forcing variables that are required to run SnowModel, (2) the historical record needed for model calibration, and (3) the relatively low latency needed to run the model in near real-time (latency of 5 days). Hourly NLDAS-2 forcing data were aggregated to 3-hourly values to correspond with the model simulation time step. The 3-hourly NLDAS-2 forcing data along with mean elevation of each NLDAS-2 grid cell were used by MicroMet to downscale and create the 30-m spatial resolution meteorological forcing data required by SnowModel [50].

This study implemented five primary configurations of SnowModel to evaluate differences and possible improvements in model performance (table A-1). The first configuration used the default SnowModel parameters without use of data assimilation (SnowModeldefault_noassim).

The SnowAssim data assimilation system was used in subsequent configurations of SnowModel in this study to assimilate daily SWE values from 17 long-term SNOTEL stations across the study domain [55]. This data assimilation procedure used comparisons between daily SWE values from each SNOTEL station to daily simulated SWE to generate precipitation and melt rate adjustment factors for each year of the simulation period that were spatially interpolated across the domain [55]. The default SnowModel parameters (with data assimilation) were also used for the second model configuration (SnowModeldefault). The third and fourth configurations of SnowModel included the calibration of SnowModel parameters (SnowModelcalibrated) and the addition of a Landsat-based precipitation correction field (SnowModelLandsat) and are described in A-2.3. Lastly, a post-processing routine to update calibrated SnowModel gridded outputs using remotely sensed SCA images was developed (SnowModelSCA_update) and is described in A-2.4.

**Table A-1.—SnowModel configurations used in this study**

| SnowModel Configuration Name | SnowModel Configuration Description |
|---|---|
| $\text{SnowModel}_{\text{default_noassim}}$ | default SnowModel parameters without data assimilation |
| $\text{SnowModel}_{\text{default}}$ | default SnowModel parameters with data assimilation of SNOwpack TELemetry Network (SNOTEL) snow water equivalent (SWE) |
| $\text{SnowModel}_{\text{calibrated}}$ | calibrated SnowModel parameters with data assimilation of SNOTEL SWE |
| $\text{SnowModel}_{\text{Landsat}}$ | calibrated SnowModel parameters with data assimilation of SNOTEL SWE and Landsat snow persistence (SP) precipitation correction field |
| $\text{SnowModel}_{\text{SCA_update}}$ | $\text{SnowModel}_{\text{Landsat}}$ gridded outputs post-processed and updated for dates corresponding with remotely sensed snow-covered area (SCA) images |

# A-2.3 Model Calibration

A calibration subdomain (32 km × 13 km) containing 5 SNOTEL stations was developed within the study area for calibrating SnowModel (SnowModelcalibrated; figure A-1) to make running time manageable. The calibration subdomain showed an elevational (median elevation of 3,196 m; figure A-S1) and land cover (68 percent forest cover) distribution that was comparable to the entire study domain (median elevation of 2,967 m, 66 percent forest cover). We used a single gridded representation of Landsat-derived mean annual snow persistence (SP; the average number of days per year that a grid cell is snow covered between January and July; Supporting Information S2) and time-series gridded data of cloud-gap-filled [64] MODIS (MOD10A1F) and VIIRS (VNP10A1F) snow-covered area (SCA; ratio of snow-covered area to total area) as the primary spatial and temporal calibration targets, respectively. Both the mean annual historical Landsat dataset and the daily cloud-gap filled MODIS and VIIRS datasets used in this study helped address possible limitations from revisit cycles and cloud cover of these observations. This multi-objective calibration approach using remotely sensed SP and SCA reduced the dependence on SNOTEL SWE observations for model validation and allowed for these ground-based SWE measurements to be assimilated into SnowModel to adjust rates of snow accumulation and melt. However, snow density observations from SNOTEL stations were

additionally used as a model calibration target. The spatial efficiency metric (SPAEF), a multiple-component (correlation, coefficient of variation and histogram overlap) evaluation metric of spatial patterns [65], was used to compare spatial patterns of SnowModel and Landsat SP. Root mean squared error (RMSE) and Nash-Sutcliffe efficiency (NSE) objective functions were used to compare MODIS/VIIRS and SnowModel daily mean SCA as well as SNOTEL snow density and SnowModel snow density across the calibration domain. A range of SnowModel parameters that define snow density evolution, wind redistribution of snow, and snow albedo were calibrated using Latin Hypercube sampling [66] in a stepwise process (table A-2). Parameter ranges were determined by previous studies [e.g., 47, 58] and expert opinion to effectively explore the parameter space. We ran 600 different uniquely parameterized SnowModel simulations on the USGS Denali Supercomputer [67] in parallel for water years 2000 through 2020. The parameter sets that maximized SPAEF and NSE and minimized RMSE were considered for the final calibrated parameters. However, parameter sets that maximized Landsat SPAEF did not always minimize MODIS RMSE; therefore, final preference was given to the parameter set that optimized the SPAEF metric in the calibration subdomain as it also resulted a comparatively low MODIS RMSE.

Subsequently, as part of the calibration effort, a grid-by-grid Landsat-based precipitation correction field was developed and applied to SnowModelcalibrated simulations to further adjust the calibrated model for biases in the meteorological forcing data (SnowModelLandsat). This precipitation correction field was developed according to the exponential relation between SP and peak SWE for all SNOTEL stations within the study domain (figure A-3). For each SNOTEL station, the mean annual SP and mean annual peak SWE were computed for water years 2000 through 2020. The normalized difference in SP (SP minus mean annual SP) and the normalized ratio of peak SWE to mean annual peak SWE were then computed by site for each water year. The normalized difference in SP was then plotted against the normalized ratio of peak SWE to mean peak SWE for all SNOTEL sites within the study area (figure A-3). This exponential relation was then used to convert the grid-by-grid difference in mean annual SP between SnowModelcalibrated and Landsat to the grid-by-grid Landsat-based precipitation correction field for the model domain. The Landsat-based precipitation correction field was applied to all SnowModelLandsat simulations.

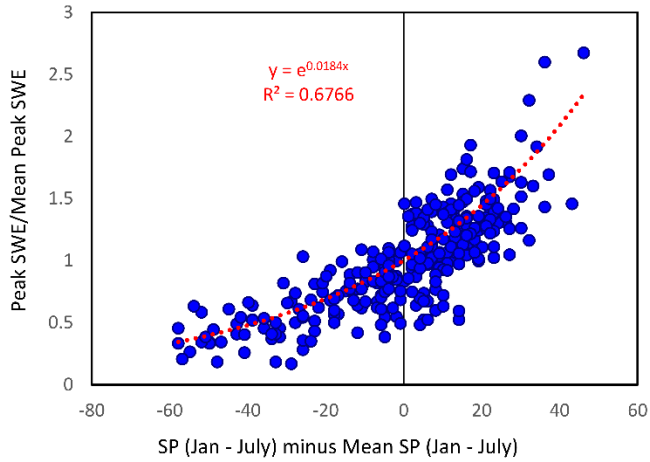


**Figure A-3.—Exponential relation developed between snow persistence (SP) and peak snow water equivalent (SWE) for all SNOTEL stations within the study domain. The relation is computed based on the site-specific normalized difference in SP (SP minus mean SP) and the site-specific normalized ratio of peak SWE to mean peak SWE [45].**

## A-2.4 SnowModel Output Grid Updates Using Remotely Sensed SCA

This study also developed a post-processing routine for SnowModel output grids to be updated with fine-resolution remotely sensed SCA data (e.g., Landsat, Sentinel-2) in support of additional real-time model applications (SnowModelSCA_update). SnowModel output grids with SWE greater than 10 millimeters (mm) were considered as snow covered [68] and compared to overlapping remotely sensed SCA for this study. For scenarios when SnowModel output grid SCA and remotely sensed SCA did not differ, no updates to the SnowModel output grids were made. For scenarios when a SnowModel output grid was simulated as snow covered but the remote sensing observation showed the grid as snow-free, the SnowModel output grid SWE for that grid cell was set to 0 mm. For scenarios when a SnowModel output grid was simulated as snow-free but the remote sensing observation showed the grid as snow-covered, the SnowModel output grid was updated with an elevation and aspect-based mean SnowModel SWE output condition computed for each basin of interest. This mean SnowModel SWE output was computed from output grid SWE values greater than 0 mm for 200 m elevation zones within north-facing, east-facing, south-facing, and west-facing aspects (figure A-2). In this study, SnowModelSCA_update (SnowModelLandsat output grids updated with remotely sensed SCA) outputs were generated only for dates that corresponded with remotely sensed SCA images.

## A2.5 Model Evaluation

The SnowModel simulations developed for this study (table A-1) were evaluated by airborne lidar derived SWE (observed snow depth and modeled snow density) datasets generated by ASO [41] during April and May 2022 and 2023 for the Colorado River at Windy Gap and Big Thompson River Basins (figure A-1). ASO SWE datasets (50 m spatial resolution) were resampled to the SnowModel grid resolution (30-m spatial resolution) using bilinear interpolation. Comparisons between mean SWE from ASO and SnowModel were made at the basin scale and by elevation zones that are commonly used for streamflow forecasts in this region (high elevations [>3,124 m], middle elevations [2,438 – 3,124 m], and low elevations [<2,438 m]) within the study area. Additionally, a grid-by-grid evaluation between ASO and SnowModel was used to evaluate mean error, mean absolute error, RMSE, percent bias, NSE, and Pearson correlation coefficient performance metrics for the SnowModel versions developed in this study. These comparisons and statistics included areas with zero or very low snow, thus evaluations across elevation zones allowed for the assessment over a range of observed SWE values. Model evaluation results were compared between the SnowModeldefault_noassim, SnowModeldefault, SnowModelcalibrated, and SnowModelLandsat configurations. Comparisons in model performance between the SnowModelLandsat and SnowModelSCA_update (SnowModelLandsat updated with remotely sensed SCA) were also made to evaluate the value added of using remotely sensed SCA in near real-time SnowModel applications. In this study, ASO remote sensing datasets were classified as snow covered if ASO-derived SWE was greater than 10 mm. Landsat fractional SCA remote sensing datasets were considered snow covered if fractional SCA was greater than 10 percent [69]. In a first step of this analysis, we used three ASO datasets collected in late May for the Shadow Mountain Basin (26 May 2022, 27 May 2023) and the Big Thompson Basin (21 May 2023) to generate SnowModelSCA_update gridded outputs and evaluate model performance. The ASO remotely sensed datasets were used to (1) compute the observed SCA, (2) update the SnowModel simulations based on these SCA observations, and (3) evaluate modeled SWE performance. In a second assessment of SnowModelLandsat and SnowModelSCA_update outputs, we used a time series of the Landsat fractional SCA images [70, 71] for observations of SCA. We evaluated the difference between SnowModelLandsat and SnowModelSCA_update outputs throughout the snow season from January through August 2010–2012 and 2018–2020 for the Shadow Mountain Basin. Landsat SCA images were only used to generate SnowModelSCA_update outputs during this period when there were less than 25% missing observations because of cloud cover.

# A-3 Results

## A-3.1 Model Calibration

The SnowModel parameters calibrated for this study are shown in table A-2. Calibration parameter adjustments generally resulted in slower snow density increases with time, greater wind speeds and resulting blowing snow redistribution and sublimation at high elevations, and lower snow albedos for both open and forested environments. SnowModelcalibrated showed a reduced RMSE for snow density and SWE at SNOTEL stations compared to SnowModeldefault_noassim (table A-S1). An example of how model performance for simulated snow density at SNOTEL stations varied with the snow density rate adjustment factor parameter is shown in figure A-S2. A comparison of SnowModel simulations to MODIS observations for time series domain wide SCA (percent of domain that is snow covered) improved RMSE from 13.3% to 11.3% during calibration (figure A-4; table A-S2). SnowModelcalibrated also showed an improved SPAEF from 0.10 to 0.22 compared to the SnowModeldefault (figure A-5; table A-S2).

A Landsat-based precipitation correction field ranging from 0.1 to 2.5 based on simulated versus observed mean annual SP was used as an additional step in the calibration process for this study (figure A-3, A-S3). The spatial field of Landsat-based precipitation correction factors applied for these SnowModelLandsat simulations is shown in figure A-S3. The Landsat-based correction field further improved SnowModelLandsat performance compared to SnowModelcalibrated for SNOTEL (table A-S1) and MODIS (figure A-4; table A-S2) data comparisons. However, SnowModelLandsat had lower overall SPAEF performance compared to SnowModelcalibrated when evaluating the spatial pattern of Landsat SP (figure A-5; table A-S2). Despite the decrease in overall SPAEF, applying the correction field to modeled precipitation substantially improves the overall correlation (α) between SnowModelLandsat and Landsat SP (figure A-5; table A-S2). Additionally, the mean bias between SnowModelLandsat and Landsat SP (-2.8 days) was lower compared to the mean bias between SnowModelcalibrated and Landsat SP (-3.7 days; figure A-5). Although SnowModelLandsat was generally shown to improve the simulation of SP, low elevation areas were generally biased low (figure A-5).

**Table A-2.—SnowModel parameters with default and final calibrated values and the ranges for each parameter that were used for the Latin Hypercube sampling [43]**

| Parameter Description (parameter name) | Calibration Step and Process | Default Value | Calibrated Value [calibration range] |
|---|---|---|---|
| Rain-snow threshold (snowfall_frac) | not calibrated | [72] | [72] |
| Snow density rate adjustment factor (ro_adjust) | step 1 snow density evolution | 5.0 | 0.4 [0.1–5.0] |

| Parameter Description (parameter name) | Calibration Step and Process | Default Value | Calibrated Value [calibration range] |
|---|---|---|---|
| Curvature length scale (curve_len_scale) | step 2 wind redistribution of snow | 500 | 575 [30–600] |
| Slope weight factor (slopewt) | step 2 wind redistribution of snow | 0.58 | 0.18 [0–1] |
| Curvature weight factor (curvewt) | step 2 wind redistribution of snow | 0.42 | 0.82 [0–1] |
| Wind increase/decrease with elevation (wind_lapse_rate) | step 2 wind redistribution of snow | 0.0 | 1.81 [1–2] |
| Forest snow albedo minimum (for_al_min) | step 3 snow albedo | 0.40 | 0.22 [0.10–0.55] |
| Open area snow albedo minimum (open_al_min) | step 3 snow albedo | 0.50 | 0.42 [0.10–0.55] |
| Forest snow albedo maximum (for_al_max) | step 3 snow albedo | 0.68 | 0.56 [0.55–0.90] |
| Open area snow albedo maximum (open_al_max) | step 3 snow albedo | 0.80 | 0.71 [0.55–0.90] |
| Forest snow albedo decay cold snow (for_al_gr_cold) | step 3 snow albedo | 0.03 | 0.02 [0.010–0.035] |
| Open area snow albedo decay cold snow (open_al_gr_cold) | step 3 snow albedo | 0.02 | 0.02 [0.010–0.035] |
| Forest snow albedo decay melting snow (for_al_gr_melt) | step 3 snow albedo | 0.06 | 0.06 [0.045–0.095] |

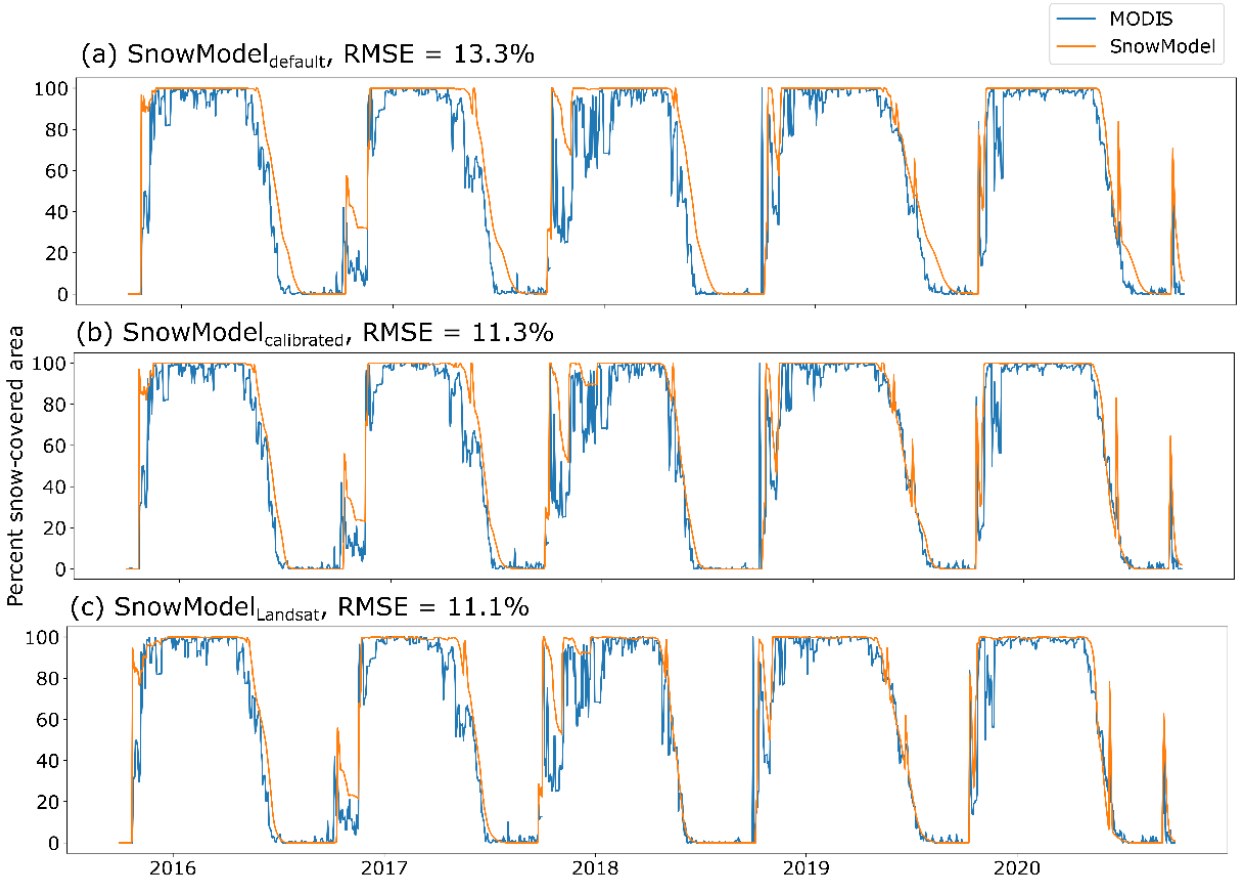


**Figure A-4.—Time series plots and root mean squared error (RMSE) statistics of daily mean percent snow covered area (SCA) across the model domain comparing MODIS observations [64] with SCA simulated by the (a) default SnowModel version (SnowModel$_{default}$), (b) calibrated SnowModel version (SnowModel$_{calibrated}$), and (c) calibrated with Landsat correction field SnowModel version (SnowModel$_{Landsat}$) for water years 2016 through 2020 [43].**

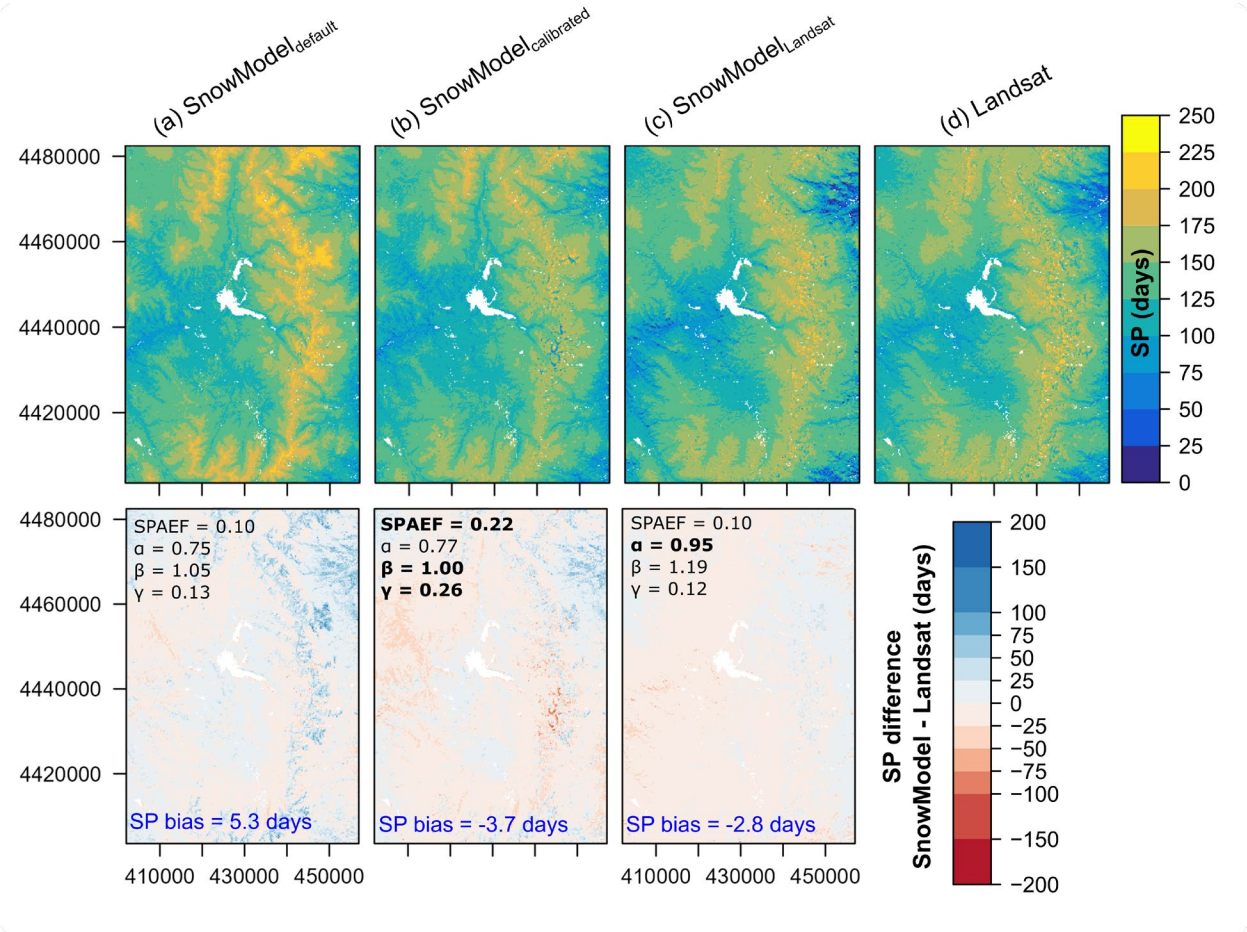


**Figure A-5.—Mean annual snow persistence (SP) and difference from Landsat-derived SP across the study area domain for water years 2000 through 2020 and the spatial efficiency metric (SPAEF) statistics (including correlation [α], ratio of coefficient of variation [β], and histogram match [γ]) [65] for the (a) default SnowModel version ($SnowModel_{default}$), (b) calibrated SnowModel version ($SnowModel_{calibrated}$), and (c) calibrated with Landsat correction field SnowModel version ($SnowModel_{Landsat}$) [43] as compared to (d) Landsat observations [71]. Mean SP bias is shown in blue text. Bolded SPAEF statistics indicate the best value.**

## A-3.2 Historical Model Version Comparisons

We evaluated differences in the four SnowModel versions developed by this study (SnowModeldefault_noassim, SnowModeldefault, SnowModelcalibrated, and SnowModelLandsat) and compared these simulations with SNOw Data Assimilation System (SNODAS) [27], a commonly used operational snow model available at 1 km spatial grid resolution (figure A-6). For comparison, the SNODAS outputs were resampled to the 30 m SnowModel spatial resolution grid. The assimilation of SNOTEL SWE data into SnowModeldefault resulted in substantial increases in SWE compared with SnowModeldefault_noassim, especially at high elevations where peak SWE was approximately 1.75 times higher. Model calibration of SnowModelcalibrated resulted in a reduction of SWE at

the high elevations as a result of increased blowing snow redistribution and sublimation as well as earlier melt out across all elevations compared to SnowModeldefault (figure A-6). SnowModelLandsat showed small increases or decreases of SWE and more gradual and later melt outs compared to the calibrated model for the middle and high elevations. Both SnowModelcalibrated and SnowModelLandsat simulated greater SWE across all elevations (especially at high and low elevations) compared to the SNODAS model. The SNODAS model showed a more rapid snowmelt rate and earlier melt out compared with SnowModel (figure A-6).

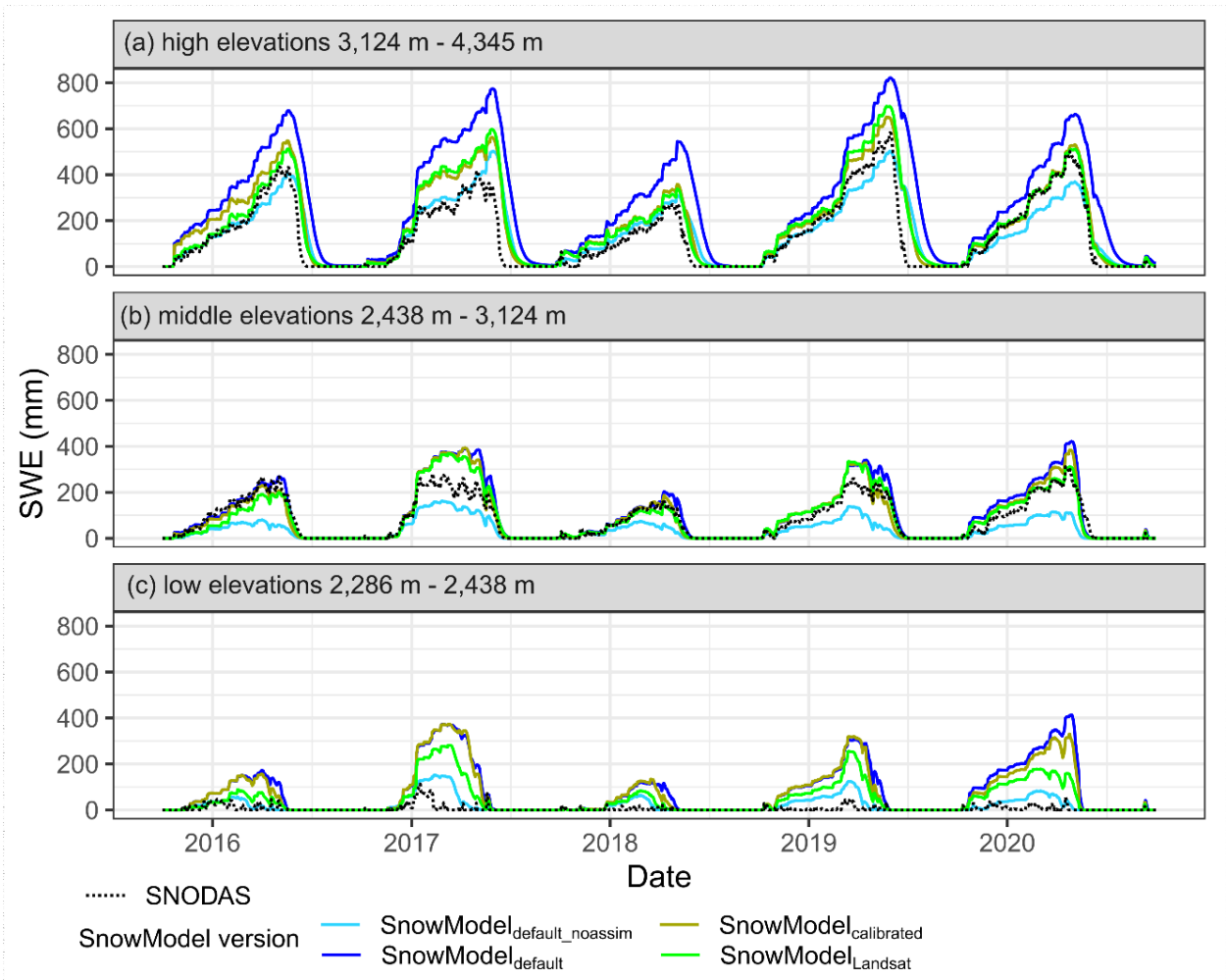


**Figure A-6.—Time series comparison plots of mean snow water equivalent (SWE) across the Big Thompson Basin for water years 2016 through 2020 simulated by the default SnowModel version without SNOTEL assimilation ($SnowModel_{default_noassim}$), default SnowModel version ($SnowModel_{default}$), calibrated SnowModel version ($SnowModel_{calibrated}$), calibrated with Landsat correction field SnowModel version ($SnowModel_{Landsat}$), and the Snow Data Assimilation (SNODAS) model for (a) high elevations, (b) middle elevations, and (c) low elevations.**

## A-3.3 Model Evaluation Comparing to ASO

On 18 April 2022 and 26 May 2022, ASO flights were collected for the Windy Gap Basin (figure A-1). Comparisons between ASO-derived SWE, SNODAS SWE, and the four SnowModel versions developed by this study (figure A-7) show improved performance of the SnowModelcalibrated (mean error ranging from 22 to 31 mm) and SnowModelLandsat (mean error ranging from -28 to -6 mm) versions compared to SNODAS (mean error ranging from 34 to 48 mm) and SnowModeldefault (mean error ranging from 69 to 86 mm). Results indicate a negative bias for the SnowModeldefault_noassim and a positive bias for the SnowModeldefault highlighting the influence of assimilating SNOTEL SWE data into the default model (figure A-7, A-8). Additionally, SnowModelLandsat showed improved error and correlation performance metrics compared to the SnowModelcalibrated (tables A-3, A-S3). The SnowModelLandsat simulated basin wide mean SWE (196 mm, 98 mm) compared well to the ASO SWE estimates (223 mm, 104 mm) on 18 April 2022 and 26 May 2022, respectively (figure A-7). The mean difference between the SnowModel SWE and ASO-derived SWE across the basin on 26 May 2022 was only −6 mm (figure A-S4), and the spatial patterns between datasets were well correlated (table S3; figure A-8). Observed errors are somewhat homogenous spatially from north to south (figure A-8d), which may indicate interannual differences in snow accumulation patterns compared to the mean annual conditions. Both SNODAS and SnowModelLandsat performed relatively well simulated the mean SWE condition across all elevation zones (tables A-3, A-S3). However, the grid-by-grid comparison of the SnowModelLandsat and ASO-derived SWE (RMSE of 137 mm and 121 mm for 18 April 2022 and 26 May 2022, respectively) showed a substantial improvement compared to the comparison of the SNODAS and ASO-derived SWE (RMSE of 193 mm and 199 mm for 18 April 2022 and 26 May 2022, respectively) across middle and high elevation zones (figure A-7, table A-3).

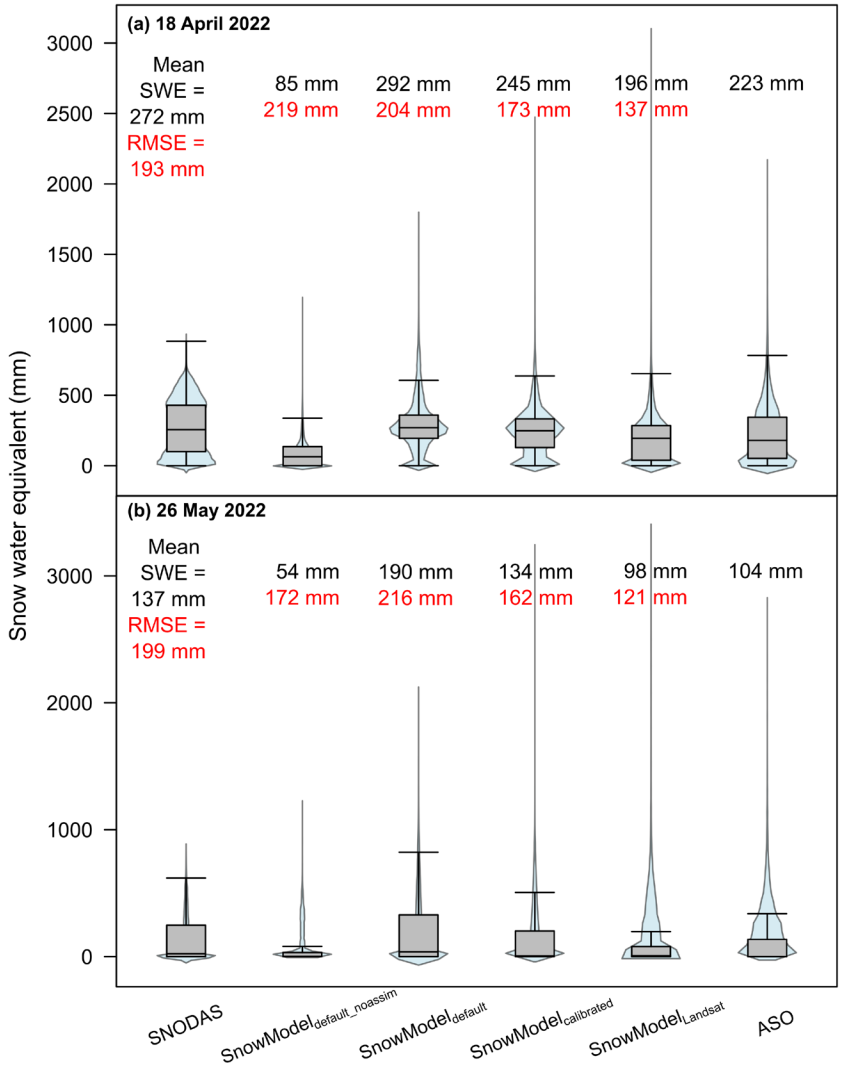


**Figure A-7.—Combination of violin plot and boxplot of simulated snow water equivalent (SWE) distribution, simulated mean SWE value, and root mean squared error (RMSE) for SNODAS, the default SnowModel version without SNOTEL assimilation ($SnowModel_{default_noassim}$), default SnowModel version ($SnowModel_{default}$), calibrated SnowModel version ($SnowModel_{calibrated}$), and calibrated with Landsat correction field SnowModel version ($SnowModel_{Landsat}$) [43] as compared to Airborne Snow Observatories (ASO)-derived SWE for (a) 18 April 2022 and (b) 26 May 2022 across the Windy Gap Basin [46].**

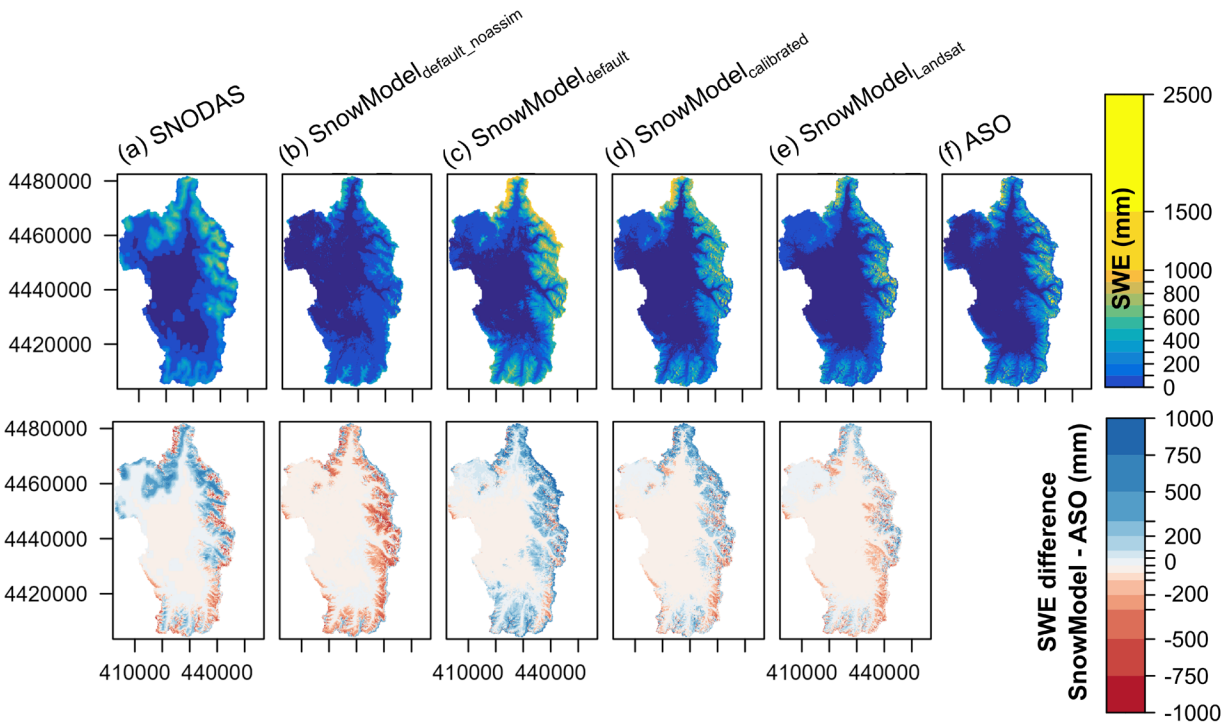


Figure A-8.—Maps of simulated snow water equivalent (SWE) distribution and difference from Airborne Snow Observatories (ASO)-derived SWE for the (a) SNODAS, (b) default SnowModel version without SNOTEL assimilation ($SnowModel_{default_noassim}$), (c) default SnowModel version ($SnowModel_{default}$), (d) calibrated SnowModel version ($SnowModel_{calibrated}$), and (e) calibrated with Landsat correction field SnowModel version ($SnowModel_{Landsat}$) [43] as compared to (f) Airborne Snow Observatories (ASO)-derived SWE for 26 May 2022 across the Windy Gap Basin [46].

**Table A-3.—Selected performance statistics [Root Mean Squared Error (RMSE) and Nash-Sutcliffe Efficiency (NSE)] based on grid-by-grid SNODAS and SnowModel [calibrated with Landsat correction field SnowModel version (SnowModelLandsat)] simulated snow water equivalent (SWE) compared to Airborne Snow Observatories (ASO)-derived SWE for the 18 April 2022 and 26 May 2022 across the Windy Gap Basin. Performance statistics are provided for all elevations, high elevations (>3,124 m), middle elevations (2,438–3,124 m), and low elevations (<2,438 m). "---" indicates zero snow observed. Additional performance statistics are provided in figure A-S4**

| Model version – All Elevation | **April 18, 2022 SNODAS** | **April 18, 2022 SnowModel$_{Landsat}$** | **May 26, 2022 SNODAS** | **May 26, 2022 SnowModel$_{Landsat}$** |
|---|---|---|---|---|
| Model mean SWE (mm) | 272 | 196 | 138 | 98 |
| ASO mean SWE (mm) | 223 | 223 | 104 | 104 |
| RMSE (mm) | 193 | 137 | 199 | 121 |
| NSE | 0.13 | 0.56 | 0.00 | 0.63 |
| Model version – High Elevation | **April 18, 2022 SNODAS** | **April 18, 2022 SnowModel$_{Landsat}$** | **May 26, 2022 SNODAS** | **May 26, 2022 SnowModel$_{Landsat}$** |
| Model mean SWE (mm) | 405 | 320 | 309 | 273 |
| ASO mean SWE (mm) | 406 | 406 | 284 | 284 |
| RMSE (mm) | 260 | 200 | 307 | 203 |
| NSE | -0.38 | 0.18 | -0.42 | 0.38 |
| Model Version Middle Elevation | **April 18, 2022 SNODAS** | **April 18, 2022 SnowModel$_{Landsat}$** | **May 26, 2022 SNODAS** | **May 26, 2022 SnowModel$_{Landsat}$** |
| Model mean SWE (mm) | 209 | 136 | 54 | 11 |
| ASO mean SWE (mm) | 135 | 135 | 14 | 14 |
| RMSE (mm) | 150 | 91 | 114 | 38 |
| NSE | -0.56 | 0.44 | -4.65 | 0.38 |
| Model Version Low Elevation | **April 18, 2022 SNODAS** | **April 18, 2022 SnowModel$_{Landsat}$** | **May 26, 2022 SNODAS** | **May 26, 2022 SnowModel$_{Landsat}$** |
| Model mean SWE (mm) | 18 | 1 | 0 | 0 |
| ASO mean SWE (mm) | 10 | 10 | 0 | 0 |
| RMSE (mm) | 20 | 23 | --- | --- |
| NSE | -0.07 | -0.36 | --- | --- |

## A-3.4 Value Added Using Additional Real-Time Remote Sensing Datasets

We evaluated if the SnowModelLandsat simulations could be further improved using remotely sensed SCA observations in a real-time framework. The mean bias of the SnowModelLandsat simulation compared to ASO for the Shadow Mountain Basin from 26 May 2022 was very small (−5 mm) and further model improvements from updating SnowModel output with the ASO SCA observations (SnowModelSCA_update) were not shown (figures A-9, A-10). However, a larger negative bias in SnowModel Landsat simulations was observed for the Shadow Mountain Basin on 27 May 2023 and the Big Thompson Basin on 21 May 2023; the SnowModelSCA_update simulations further reduce these mean biases from −61 mm to −28 mm and from −23 mm to

−5 mm, respectively (figures A-9, A-10). For all three dates evaluated, the greatest reductions in bias were found for the middle elevation zones between 3,000 m and 3,300 m, which were slightly above the snow line during that time of year (figures A-9, A-10).

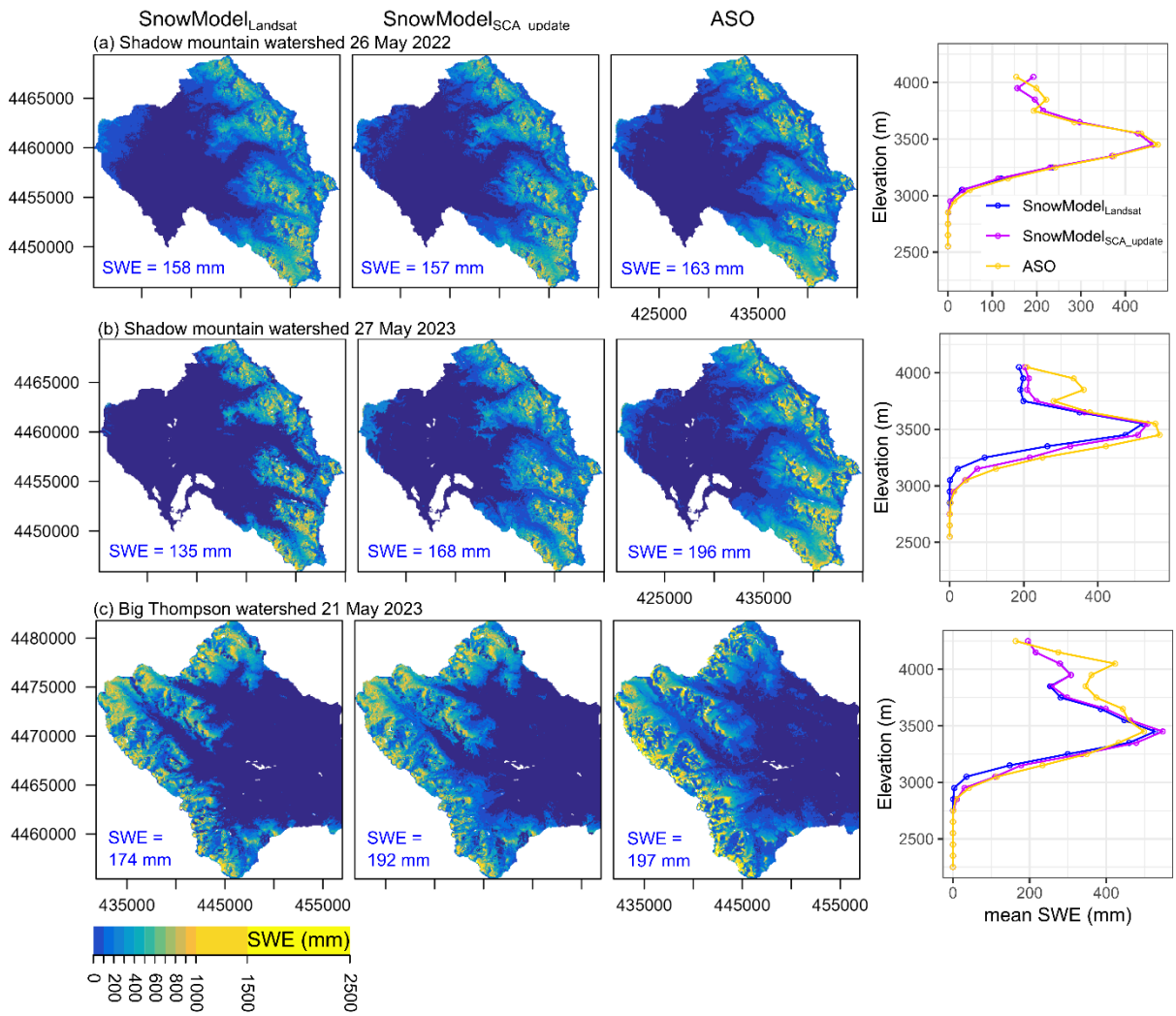


**Figure A-9.—Map and elevation-based comparison of snow water equivalent (SWE) distribution between SnowModel$_{Landsat}$, SnowModel$_{SCA_update}$ [43], and Airborne Snow Observatories (ASO) for the (a) Shadow Mountain Basin on 26 May 2022, (b) Shadow Mountain Basin on 27 May 2023, and (c) Big Thompson Basin on 21 May 2023 [46].**

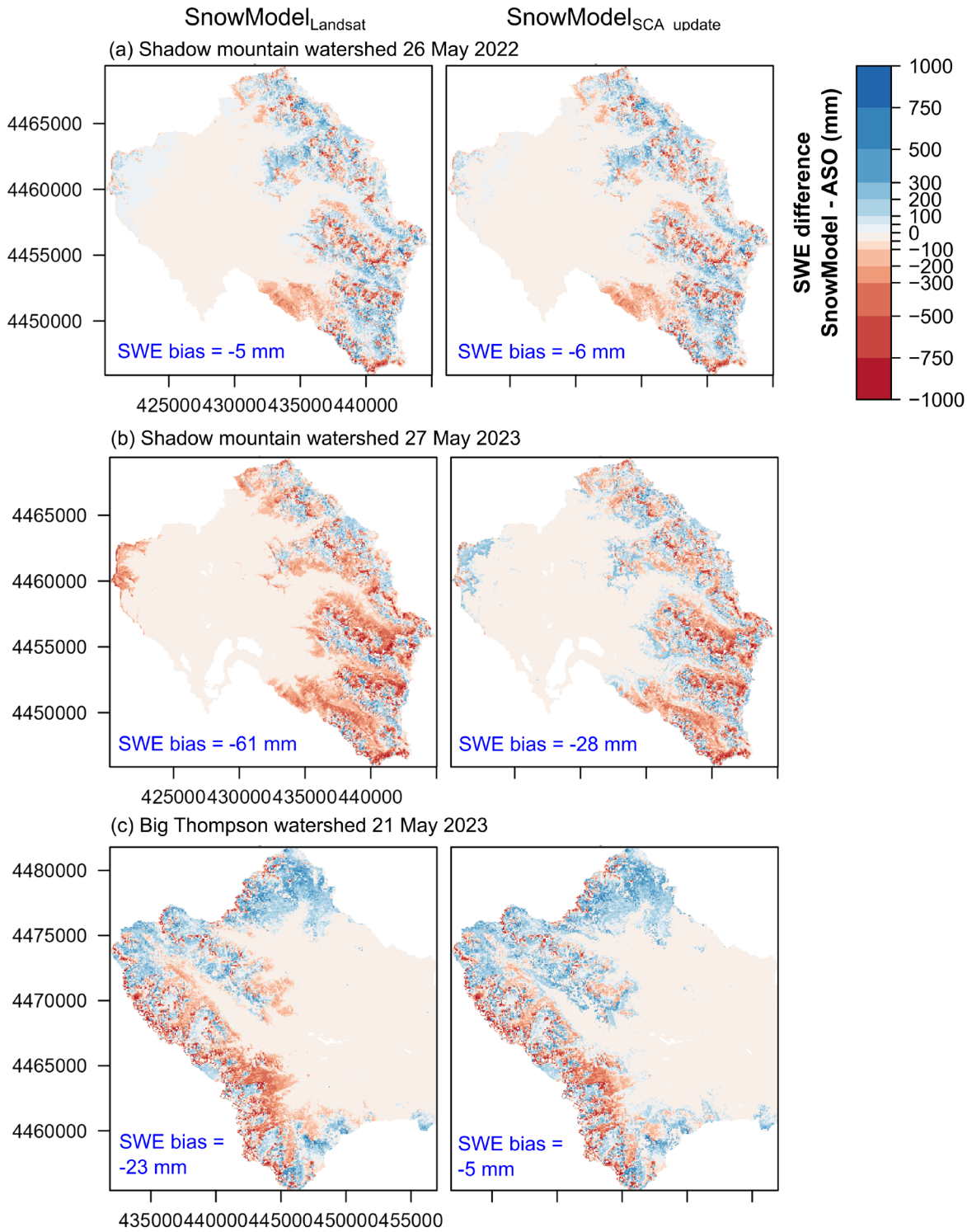


**Figure A-10.—Map of snow water equivalent (SWE) distribution difference from Airborne Snow Observatories (ASO)-derived SWE for SnowModel$_{Landsat}$ and SnowModel$_{SCA_update}$ [43] for the (a) Shadow Mountain Basin on 26 May 2022, (b) Shadow Mountain Basin on 27 May 2023, and (c) Big Thompson Basin on 21 May 2023 [46].**

Landsat fractional SCA data [70, 71] of the Shadow Mountain Basin from January through August (2010–2012 and 2018–2020) included 31 percent (n = 67) of images with less than 25 percent missing grid cells because of cloud cover. Comparisons between SnowModelLandsat and SnowModelSCA_update using this time series of images showed that the basin mean absolute difference across all images was small (7 mm; figure A-11). However, basin mean differences between the model versions were as large as −82 mm. The percentage difference between SnowModelLandsat and SnowModelSCA_update was generally greater than 5% during January, May, June, July, and August, indicating this technique is likely most useful during the early accumulation and snowmelt season (figure A-11).

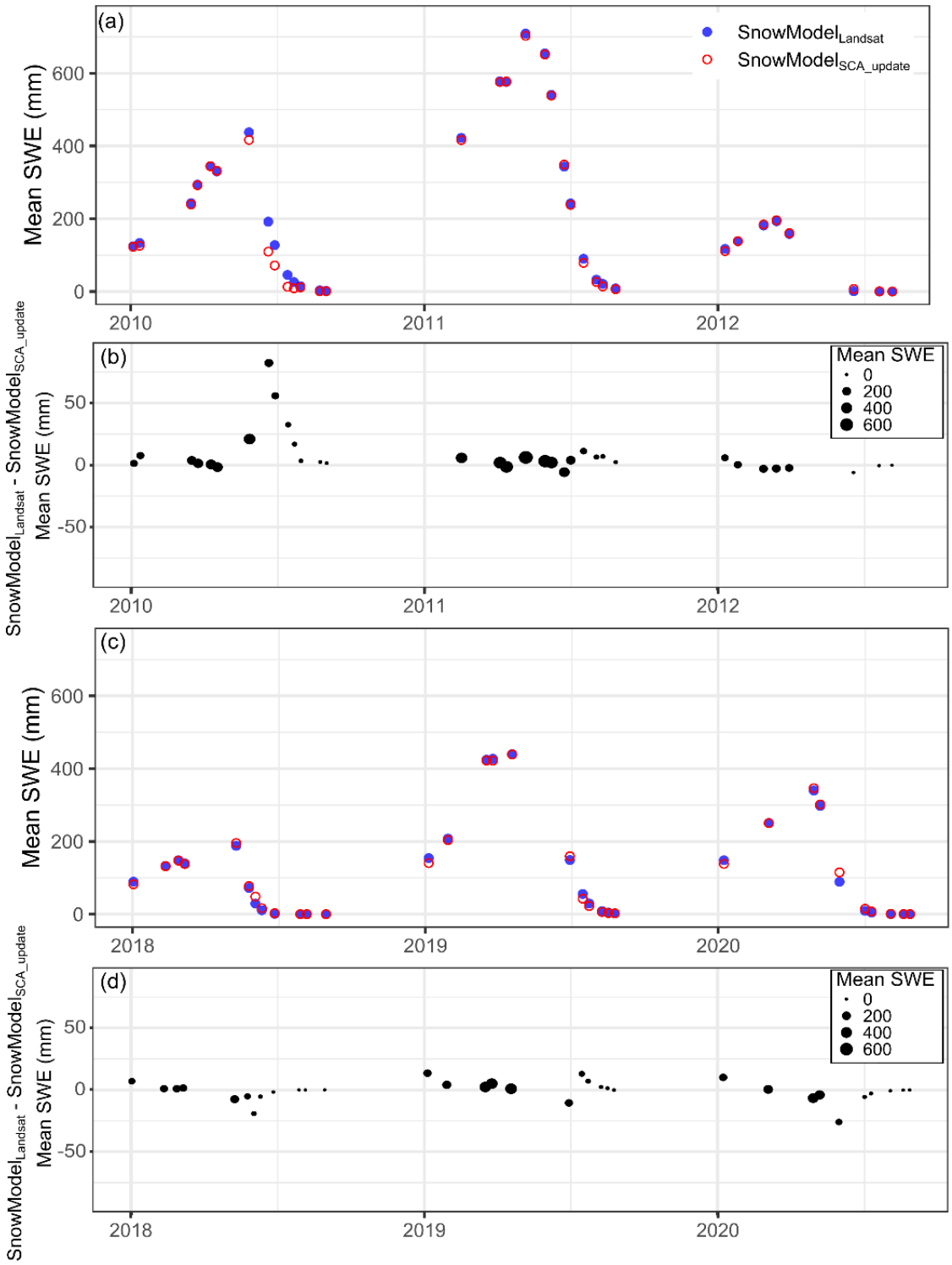


Figure A-11.—Time series comparison (a, c) and difference (b, d) of mean snow water equivalent (SWE) of the Shadow Mountain Basin from dates corresponding with Landsat SCA observations (January through August) between SnowModel$_{Landsat}$ and SnowModel$_{SCA_update}$ for (a, b) water years 2010 through 2012 and (c, d) water years 2018 through 2020 [43].

# A-4 Discussion

## A-4.1 Advantages of Near Real-Time Spatially Distributed Snow Modeling Approach

Key results of this study highlight that information from fine spatial resolution (30 m) and high temporal resolution (daily) remotely sensed snow cover can support important improvements to process-based snow modeling simulations that can be run in near real-time. In complex mountainous environments, patterns of mean annual SP observed by Landsat highlight important repeatable snow holding patterns across the landscape [73], and this information was used as a valuable spatial calibration target for the snow modeling performed in this study (figure A-5). A time series of domain-wide MODIS/VIIRS daily SCA observations was also used as an important temporal calibration target that was particularly important for better representing snowmelt timing (figure A-4). Furthermore, our results show that the strong relation between SP and peak SWE [69, 74, 75] can be leveraged to further constrain and bias-correct precipitation forcing patterns for process-based snow modeling (figures A-7, A-8). This result is consistent with the many studies that have highlighted how snow patterns across the landscape tend to be temporally consistent from year to year [76–80]. Results from this study also highlight that post-processing of SnowModel gridded outputs with observed fine resolution SCA (e.g., from Landsat or Sentinel 2) can further refine process-based snow model SWE estimates; these updates were shown to have the greatest influence on SWE estimates (figure A-9, A-11) at or near snow line elevations during the early accumulation and late snowmelt seasons [32, 81]. Taken together, these results present a new approach to calibrate and post-process a process-based snow model that can be applied in near real time using fine spatial resolution and high temporal resolution remotely sensed snow-cover information.

Process-based snow modeling at fine spatial resolutions using the approach outlined in this study has important advantages for the development of additional near real-time SWE estimations. This modeling approach includes the first-order processes governing the seasonal evolution of the snowpack that could be able to represent varying sensitivities to future climate-induced changes to the snowpack energy balance [8, 82–84]. Furthermore, the fine spatial resolution of the model grid allows for a more realistic representation of the topographic influence on snow process dynamics [85, 86]. The SnowModel simulations developed in this study importantly capture the complex snow patterns (figure A-9) and a more gradual snowmelt rate (figure A-6) at the highest elevations. These snow dynamics are driven by deep pockets of wind redistributed snow and were more accurately simulated because of the incorporation of remotely sensed snow cover data into the model development. The comparison of high elevation SWE shown in figures A-6a and A-8 highlights the contrast between the rapid depletion of snow simulated by the coarser SNODAS model with the more gradual late season snowmelt simulated by SnowModelLandsat. More accurate quantification of late season high elevation snow water storage and variability (table A-3) and snowmelt runoff can be important for the management of inflow forecasts to reservoirs in high-elevation basins. The near real-time modeling approach

presented in this study fills an important need that can support additional snow and water supply forecasting, and can be applied with available fine-resolution remote sensing datasets [87, 88] anywhere on earth.

## A-4.2 Comparisons to previous investigations

To put the results of this study in context with previous investigations, we compared model performance statistics computed by this work to other SWE estimation studies that have compared results to ASO datasets. SnowModel simulations calibrated for the Rio Grande headwaters [58] at a 100-m spatial resolution showed a grid-by-grid RMSE of 159 mm when comparing to an ASO flight around peak snow accumulation. Results presented in this study show comparable but improved performance statistics from Sexstone et al. [58] with comparisons to ASO highlighting RMSE values from 121 to 137 mm (figure A-S4). Other recent process-based modeling studies have also presented comparisons to ASO but have focused their results on comparisons of snow depth rather than SWE [40,89]. Bair, et al. [90] developed two reconstruction models for basins in the Sierra Nevada, California that compared favorably with ASO (25 and 26 mm mean absolute error). Furthermore, Yang et al. [24] developed a retrospective model combined with additional statistical techniques in the same study area to develop a real-time SWE estimation approach; results from this study highlighted a median RMSE of 133 mm from comparisons with ASO. Importantly, results from Bair et al. [90] and Yang et al. [24] were presented based on a 500 m spatial resolution. However, they are still generally comparable to the performance statistics presented by this study. Dawson, et al. [91] compared results from the 4 km spatial resolution University of Arizona SWE product [92] to ASO averaged across the basin scale in California and found a mean absolute error of 52 mm. When computed based on a 30-m grid comparison, results from this study showed a mean absolute error ranging from 54 to 87 mm. However, when averaged at the basin scale, the mean absolute error from two flight comparisons is 17 mm (figure A-S4).

## A-4.3 Temporal Consistency of Snow Patterns

This study implemented a spatial precipitation correction field in model simulations that builds off previous research highlighting how the temporal consistency of snow patterns across the landscape can be used to improve snow estimates. The data assimilation scheme SnowAssim [55] developed for SnowModel was built on the premise that observations of snow can be used to help reduce model uncertainty associated with biases in model forcing (e.g., precipitation, wind) or process representation (e.g., blowing snow redistribution). Sturm and Wagner [76] used empirically derived snow distribution patterns derived from repeated snow surveys to improve SnowModel simulations by up to 60%. Additionally, Vögeli et al. [77] used maps of snow depth distributions from digital photogrammetry to scale precipitation input data to the Alpine3D snow model [93], showing a reduction in snow depth error by a factor of 3.4. Recent work has also highlighted that snow patterns derived from historical aerial lidar snow depth surveys can be used to accurately infer snow depth patterns and snow deposition downscaling [78, 94], although important challenges were highlighted associated with seasons exhibiting abnormal snow

accumulation, mid-winter ablation, and snowmelt conditions. Despite the overall improvements in the SnowModelLandsat simulations using the Landsat SP pattern correction field in this study, we highlight errors using this approach that are homogenous spatially (figure A-8d), which may indicate similar challenges associated with interannual differences in snow accumulation patterns. Previous research has mainly used measurements of SWE or snow depth to evaluate spatial corrections of snow distributions in process-based snow modeling. However, similar to Hammond et al. [74] and Trujillo and Molotch [75], we showed that SP is well correlated with peak SWE, and we developed a relation between SP and peak SWE (figure A-3) that was used to scale precipitation inputs into SnowModel based on a similar approach presented by Vögeli et al. [77] and Raleigh and Deems [37] that was able to further reduce SnowModel RMSE by 36–41 mm from the calibrated model version (figure A-S4). As noted by Wayand et al. [73], patterns of SP from fine resolution SCA are globally scalable. Therefore, additional research would be useful that evaluates how the relation between SP and peak SWE amount across different snow regimes [75] can support linkages between SP and SWE patterns to improve process-based snow modeling and downscaling.

## A-4.4 Uncertainties and Future Research

Major uncertainties in process-based snow modeling are often associated with the uncertainties from atmospheric forcing datasets [38]. In this study, we observed a low bias in precipitation and wind speeds from the NLDAS-2 forcing data, which have been similarly observed by previous studies [95, 96]. The calibration, precipitation scaling, and data assimilation model results developed in this study are importantly specific to the atmospheric forcing dataset used (NLDAS-2 in this application) and its inherent biases. However, the peak SWE and SP relation used for precipitation scaling is likely transferable because it is solely based on observations. The approaches developed in the model workflow attempt to reduce forcing-based model uncertainties. Therefore, if major changes were made to the atmospheric forcing dataset, or a different atmospheric forcing dataset were used in the future, the model calibration and precipitation correction field would need to be redeveloped specifically to the new forcing dataset. Future research testing the model workflow developed by this study using a range of atmospheric forcing datasets could provide important information about the consistency between forcing-based and model process-based uncertainties. Additionally, future improvements in the spatial resolution, accuracy, and latency of atmospheric forcing datasets, and similarly, improvements in spatial resolution and revisit cycles of remotely sensed snow cover products could be utilized in future process-based snow modeling applications with the modeling workflow presented by this study.

This study used ASO SWE estimates as the primary evaluation dataset of the SnowModel results, and it has been shown that the majority of the uncertainty in lidar-derived SWE estimation techniques is associated with snowpack density modeling [97]. However, the magnitude of ASO product SWE uncertainty is far less than other SWE estimation techniques presented by other studies [41]. Evaluating differences between ASO and SnowModel snow density modeling approaches was outside of the scope of this research, but future research

evaluating differences and uncertainties in process-based snow modeling of snow density and their importance in real-time snow estimation could be explored.

Future research could build upon the SnowModel calibration procedure that has been developed in this study. Process-based snow models such as SnowModel are not typically calibrated using automated methods given the computational expense of this process and relatively good model performance without these procedures [e.g., 8, 15, 30, 56–58]. However, this study highlights how automated calibration procedures can improve SnowModel performance from baseline conditions (figure A-8, figure A-S4). The use of a single calibration subdomain in this study may have limited the generalizability of the model; thus, future research could consider how to use a greater number of calibration subdomains across a similar large study area. Additionally, we suggest that future research could explore a sensitivity analysis of calibrated parameters to better understand the significance of each of the calibrated parameters within the calibration process. Lastly, as more airborne lidar-derived snow products become available, future research could analyze the robustness of this type of calibration method over several years with varying climate conditions.

# A-5 Conclusions

SnowModel simulations were developed during a 24-year period (2000–2023) at 30-m spatial grid resolution across a 4,212 km2 model domain in the north-central Colorado Rocky Mountains. NLDAS-2 reanalysis was utilized for model atmospheric forcing data, and SNOTEL SWE observations were incorporated via data assimilation. SnowModel was calibrated spatially to Landsat mean annual SP and temporally to MODIS/VIIRS mean basin SCA using a multi-objective calibration procedure explored through Latin hypercube sampling and a stepwise calibration process. Landsat mean annual SP was also used to further optimize SnowModel simulations through the development of a spatially variable precipitation correction field. This study additionally developed a near real-time workflow for SnowModel simulations that includes post processing corrections of model outputs to observed fine-resolution SCA information. Evaluations of SnowModel simulations using lidar-derived ASO SWE estimates highlight that the version of SnowModel calibrated to remotely sensed SCA had improved performance compared with baseline simulations and comparable spatial patterns to ASO, especially at the highest elevations. Grid-by-grid comparisons of the baseline and final calibrated SnowModel simulations to ASO-derived SWE showed an improvement in mean RMSE from 210 mm to 129 mm, respectively. Furthermore, post-processing corrections of SnowModel gridded outputs to observed fine-resolution SCA was shown to further improve model accuracy, having the greatest influence on SWE estimates at or near snow line elevations during the early accumulation and late snowmelt seasons. Results presented in this study highlight a new approach that can be used for calibrating and post-processing a process-based snow model and can be applied in near real time using fine resolution snow-cover information. This research has potential for informing additional assessments, management planning, and water resources forecasting by providing improvements in near real-time snow water storage estimates within seasonally snow-covered mountainous environments.

**Supplementary Materials**: The following supporting information can be downloaded at: www.mdpi.com/xxx/s1, Supporting Information S1, S2; figures A-S1-A-S4; tables A-S1-A-S2.

**Author Contributions:** Conceptualization, G.S., D.S., C.L., and E.C; methodology G.S., G.A., D.S., T.B.; software, G.S., G.A., and, T.B.; validation, G.S., G.A., and D.S.; formal analysis, G.S., G.A., D.S., and T.B.; investigation, G.S., G.A., D.S., T.B., D.R., C.L., E.C, and L.B.; resources, G.S., G.A., D.S., T.B., D.R., C.L., E.C, and L.B.; data curation, G.S., G.A., D.S., T.B., and D.R.; writing—original draft preparation, G.S., G.A., D.S., T.B., D.R., C.L., E.C, and L.B.; writing—review and editing, G.S., G.A., D.S., T.B., D.R., C.L., E.C, and L.B.; visualization, G.S., G.A., D.S., T.B., and D.R.; supervision, G.S., C.L., and E.C; project administration, G.S., C.L., E.C, and L.B.; funding acquisition, G.S., D.S., C.L., and E.C. All authors have read and agreed to the published version of the manuscript.

**Funding:** This research was funded by the Bureau of Reclamation Science and Technology Program and Snow Water Supply Forecast Program and by Northern Colorado Water Conservancy District (Northern Water). Additional funding support was provided by the U.S. Geological Survey (USGS) Water Availability and Use Science Program as part of the Water Resources Mission Area Snow Hydrology Research Project and the USGS Ecosystems Land Change Science Program. Funding for Airborne Snow Observatories (ASO) data collection within the Windy Gap domain used in this study was provided by the USGS Next Generation Water Observing System (NGWOS) Program and Northern Water.

**Data Availability Statement:** The SnowModel output, land cover grids, and DEM used for this analysis are available via Akie et al. [43] and from publicly available sources cited in the text. Airborne Snow Observatories (ASO) datasets are also openly available [46].

**Acknowledgments:** Computing resources were provided by USGS Core Science Systems Advanced Research Computing Center on the Denali and Tallgrass supercomputers [67]. We would like to thank Glen Liston for providing the SnowModel code used in this study [49]. Any use of trade, firm, or product names is for descriptive purposes only and does not imply endorsement by the U.S. Government.

**Conflicts of Interest:** The authors declare no conflicts of interest.

# References

[1] Li, D.; Wrzesien, M.L.; Durand, M.; Adam, J.; Lettenmaier, D.P. How much runoff originates as snow in the western United States, and how will that change in the future? *Geophysical Research Letters* **2017**, 44, 6163-6172, doi:10.1002/2017gl073551.

[2] Lukas, J.; Payton, E. Colorado River Basin Climate and Hydrology: State of the Science; Western Water Assessment, University of Colorado Boulder: **2020**, https://doi.org/10.25810/3hcv-w477.

[3] Barnett, T.P.; Adam, J.C.; Lettenmaier, D.P. Potential impacts of a warming climate on water availability in snow-dominated regions. *Nature* **2005**, 438, 303–309, doi:10.1038/nature04141.

[4] Pagano, T.; Garen, D.; Sorooshian, S. Evaluation of Official Western U.S. Seasonal Water Supply Outlooks, 1922–2002. *J Hydrometeorol* **2004**, 5, 896–909, doi:10.1175/1525-7541(2004)005<0896:Eoowus>2.0.Co;2.

[5] Wheeler, K.G.; Udall, B.; Wang, J.; Kuhn, E.; Salehabadi, H.; Schmidt, J.C. What will it take to stabilize the Colorado River? *Science* **2022**, 377, 373–375, doi:10.1126/science.abo4452.

[6] Richter, B.D.; Lamsal, G.; Marston, L.; Dhakal, S.; Sangha, L.S.; Rushforth, R.R.; Wei, D.Y.; Ruddell, B.L.; Davis, K.F.; Hernandez-Cruz, A.; et al. New water accounting reveals why the Colorado River no longer reaches the sea. *Communications Earth & Environment* **2024**, 5, 134, doi:10.1038/s43247-024-01291-0.

[7] Bales, R.C.; Molotch, N.P.; Painter, T.H.; Dettinger, M.D.; Rice, R.; Dozier, J. Mountain hydrology of the western United States. *Water Resour Res* **2006**, 42, doi: 10.1029/2005wr004387.

[8] Hammond, J.C.; Sexstone, G.A.; Putman, A.L.; Barnhart, T.B.; Rey, D.M.; Driscoll, J.M.; Liston, G.E.; Rasmussen, K.L.; McGrath, D.; Fassnacht, S.R.; et al. High Resolution SnowModel Simulations Reveal Future Elevation-Dependent Snow Loss and Earlier, Flashier Surface Water Input for the Upper Colorado River Basin. *Earth's Future* **2023**, 11, doi:10.1029/2022ef003092.

[9] Fassnacht, S.R.; Venable, N.B.H.; McGrath, D.; Patterson, G.G. Sub-Seasonal Snowpack Trends in the Rocky Mountain National Park Area, Colorado, USA. *Water* **2018**, 10, 562, doi:10.3390/w10050562.

[10] Mote, P.W.; Li, S.H.; Lettenmaier, D.P.; Xiao, M.; Engel, R. Dramatic declines in snowpack in the western US. *Npj Climate and Atmospheric Science* **2018**, 1, 2, doi:10.1038/s41612-018-0012-1.

[11] López-Moreno, J.I.; Revuelto, J.; Fassnacht, S.R.; Azorín-Molina, C.; Vicente-Serrano, S.M.; Morán-Tejeda, E.; Sexstone, G.A. Snowpack variability across various spatio-temporal resolutions. *Hydrol Process* **2015**, 29, 1213–1224, doi:10.1002/hyp.10245.

[12] Sexstone, G.A.; Fassnacht, S.R.; López-Moreno, J.I.; Hiemstra, C.A. Subgrid snow depth coefficient of variation spanning alpine to sub-alpine mountainous terrain. *Cuadernos de*

*Investigación Geográfica* (*Geographical Research Letters*) **2022**, 48, 79–96, doi:10.18172/cig.4951.

[13] Elder, K.; Dozier, J.; Michaelsen, J. Snow Accumulation and Distribution in an Alpine Watershed. *Water Resour Res* **1991**, 27, 1541–1552, doi:10.1029/91wr00506.

[14] Egli, L.; Jonas, T. Hysteretic dynamics of seasonal snow depth distribution in the Swiss Alps. *Geophysical Research Letters* **2009**, 36, doi:10.1029/2008gl035545.

[15] Sexstone, G.A.; Clow, D.W.; Fassnacht, S.R.; Liston, G.E.; Hiemstra, C.A.; Knowles, J.F.; Penn, C.A. Snow Sublimation in Mountain Environments and Its Sensitivity to Forest Disturbance and Climate Warming. *Water Resour Res* **2018**, 54, 1191–1211, doi:10.1002/2017wr021172.

[16] Fleming, S.W.; Zukiewicz, L.; Strobel, M.L.; Hofman, H.; Goodbody, A.G. SNOTEL, the Soil Climate Analysis Network, and water supply forecasting at the Natural Resources Conservation Service: Past, present, and future. *JAWRA Journal of the American Water Resources Association* **2023**, 59, 585–599, doi:10.1111/1752-1688.13104.

[17] Sexstone, G.A.; Fassnacht, S.R. What drives basin scale spatial variability of snowpack properties in northern Colorado? *Cryosphere* **2014**, 8, 329–344, doi:10.5194/tc-8-329-2014.

[18] Gleason, K.E.; Nolin, A.W.; Roth, T.R. Developing a representative snow-monitoring network in a forested mountain watershed. *Hydrol Earth Syst Sc* **2017**, 21, 1137–1147, doi:10.5194/hess-21-1137-2017.

[19] Meromy, L.; Molotch, N.P.; Link, T.E.; Fassnacht, S.R.; Rice, R. Subgrid variability of snow water equivalent at operational snow stations in the western USA. *Hydrol Process* **2013**, 27, 2383–2400, doi:10.1002/hyp.9355.

[20] Molotch, N.P.; Bales, R.C. Scaling snow observations from the point to the grid element: Implications for observation network design. *Water Resour Res* **2005**, 41, doi:10.1029/2005wr004229.

[21] Fang, Y.; Liu, Y.; Margulis, S.A. A western United States snow reanalysis dataset over the Landsat era from water years 1985 to 2021. *Sci Data* **2022**, 9, 677, doi:10.1038/s41597-022-01768-7.

[22] Margulis, S.A.; Cortés, G.; Girotto, M.; Durand, M. A Landsat-Era Sierra Nevada Snow Reanalysis (1985–2015). *J Hydrometeorol* **2016**, 17, 1203–1221, doi:10.1175/jhm-d-15-0177.1.

[23] Smyth, E.J.; Raleigh, M.S.; Small, E.E. Improving SWE Estimation With Data Assimilation: The Influence of Snow Depth Observation Timing and Uncertainty. *Water Resour Res* **2020**, 56, e2019WR026853, doi:10.1029/2019wr026853.

[24] Yang, K.H.; Musselman, K.N.; Rittger, K.; Margulis, S.A.; Painter, T.H.; Molotch, N.P. Combining ground-based and remotely sensed snow data in a linear regression model for real-time estimation of snow water equivalent. *Advances in Water Resources* **2022**, 160, 104075, doi:10.1016/j.advwatres.2021.104075.

[25] Bair, E.H.; Calfa, A.A.; Rittger, K.; Dozier, J. Using machine learning for real-time estimates of snow water equivalent in the watersheds of Afghanistan. *Cryosphere* **2018**, 12, 1579–1594, doi:10.5194/tc-12-1579-2018.

[26] Schneider, D.; Molotch, N.P. Real-time estimation of snow water equivalent in the Upper Colorado River Basin using MODIS-based SWE Reconstructions and SNOTEL data. *Water Resour Res* **2016**, 52, 7892–7910, doi:10.1002/2016wr019067.

[27] Carroll, T.; Cline, D.; Olheiser, C.; Rost, A.; Nilsson, A.; Fall, G.; Bovitz, C.; Li, L. NOAA's national snow analyses. In Proceedings of the 74th annual meeting of the western snow conference, **2006**; p. 13, Western Snow Conference. Las Cruces, NM.

[28] Clow, D.W.; Nanus, L.; Verdin, K.L.; Schmidt, J. Evaluation of SNODAS snow depth and snow water equivalent estimates for the Colorado Rocky Mountains, USA. *Hydrol Process* **2012**, 26, 2583–2591, doi:10.1002/hyp.9385.

[29] Hedrick, A.; Marshall, H.P.; Winstral, A.; Elder, K.; Yueh, S.; Cline, D. Independent evaluation of the SNODAS snow depth product using regional-scale lidar-derived measurements. *The Cryosphere* **2015**, 9, 13–23, doi:10.5194/tc-9-13-2015.

[30] Barnhart, T.B.; Putman, A.L.; Heldmyer, A.J.; Rey, D.M.; Hammond, J.C.; Driscoll, J.M.; Sexstone, G.A. Evaluating Distributed Snow Model Resolution and Meteorology Parameterizations Against Streamflow Observations: Finer Is Not Always Better. *Water Resour Res* **2024**, 60, doi:10.1029/2023wr035982.

[31] Largeron, C.; Dumont, M.; Morin, S.; Boone, A.; Lafaysse, M.; Metref, S.; Cosme, E.; Jonas, T.; Winstral, A.; Margulis, S.A. Toward Snow Cover Estimation in Mountainous Areas Using Modern Data Assimilation Methods: A Review. *Frontiers in Earth Science* **2020**, 8, doi:10.3389/feart.2020.00325.

[32] Andreadis, K.M.; Lettenmaier, D.P. Assimilating remotely sensed snow observations into a macroscale hydrology model. *Advances in Water Resources* **2006**, 29, 872–886, doi:10.1016/j.advwatres.2005.08.004.

[33] Fletcher, S.J.; Liston, G.E.; Hiemstra, C.A.; Miller, S.D. Assimilating MODIS and AMSR-E Snow Observations in a Snow Evolution Model. *J Hydrometeorol* **2012**, 13, 1475–1492, doi:10.1175/jhm-d-11-082.1.

[34] Stigter, E.E.; Wanders, N.; Saloranta, T.M.; Shea, J.M.; Bierkens, M.F.P.; Immerzeel, W.W. Assimilation of snow cover and snow depth into a snow model to estimate snow water equivalent and snowmelt runoff in a Himalayan catchment. *The Cryosphere* **2017**, 11, 1647–1664, doi:10.5194/tc-11-1647-2017.

[35] Thirel, G.; Salamon, P.; Burek, P.; Kalas, M. Assimilation of MODIS Snow Cover Area Data in a Distributed Hydrological Model Using the Particle Filter. *Remote Sens* **2013**, 5, 5825-5850, https://doi.org/10.3390/rs5115825.

[36] Baba, M.W.; Gascoin, S.; Hanich, L. Assimilation of Sentinel-2 Data into a Snowpack Model in the High Atlas of Morocco. Remote Sens-Basel **2018**, 10, 1982, https://doi.org/10.3390/rs10121982.

[37] Raleigh, M.S.; Deems, J.S. Filling the Holes in the Space-Time Cube of Snowpack Evolution with Lasers, Cameras, Computers, and Snow Shovels. In Proceedings of the 86th Annual Western Snow Conference. Albuquerque, New Mexico **2018**.

[38] Raleigh, M.S.; Lundquist, J.D.; Clark, M.P. Exploring the impact of forcing error characteristics on physically based snow simulations within a global sensitivity analysis framework. *Hydrol Earth Syst Sc* **2015**, 19, 3153–3179, doi:10.5194/hess-19-3153-2015.

[39] Deems, J.S.; Painter, T.H.; Finnegan, D.C. Lidar measurement of snow depth: a review. *J Glaciol* **2017**, 59, 467–479, doi:10.3189/2013JoG12J154.

[40] Hedrick, A.R.; Marks, D.; Havens, S.; Robertson, M.; Johnson, M.; Sandusky, M.; Marshall, H.P.; Kormos, P.R.; Bormann, K.J.; Painter, T.H. Direct Insertion of NASA Airborne Snow Observatory-Derived Snow Depth Time Series Into the iSnobal Energy Balance Snow Model. *Water Resour Res* **2018**, 54, 8045–8063, doi:10.1029/2018wr023190.

[41] Painter, T.H.; Berisford, D.F.; Boardman, J.W.; Bormann, K.J.; Deems, J.S.; Gehrke, F.; Hedrick, A.; Joyce, M.; Laidlaw, R.; Marks, D. The Airborne Snow Observatory: Fusion of scanning lidar, imaging spectrometer, and physically-based modeling for mapping snow water equivalent and snow albedo. *Remote Sensing of Environment* **2016**, 184, 139–152.

[42] Yang, K.; Rittger, K.; Musselman, K.N.; Bair, E.H.; Dozier, J.; Margulis, S.A.; Painter, T.H.; Molotch, N.P. Intercomparison of snow water equivalent products in the Sierra Nevada California using airborne snow observatory data and ground observations. *Frontiers in Earth Science* **2023**, 11, doi:10.3389/feart.2023.1106621.

[43] Akie, G.A.; Barnhart, T.B.; Selkowitz, D.; Sexstone, G.A. Historical simulated snowpack for the Willow Creek and Big Thompson, CO watersheds and vicinity, water years 1994–2023. *U.S. Geological Survey Data Release* **2025**, https://doi.org/10.5066/P9NTGM51.

[44] MTBS. Monitoring Trends in Burn Severity (MTBS). **2024**, URL https://mtbs.gov/ (accessed 3.1.24).

[45] NRCS. Natural Resources Conservation Service (NRCS) Snow and Water Interactive Map. **2024**, URL https://www.nrcs.usda.gov/resources/data-and-reports/snow-and-water-interactive-map (accessed 3.1.24).

[46] ASO. Airborne Snow Observatories (ASO). **2024**, URL https://data.airbornesnowobservatories.com/ (accessed 3.1.24).

[47] Liston, G.E.; Elder, K. A distributed snow-evolution modeling system (SnowModel). *J Hydrometeorol* **2006**, 7, 1259–1276, doi:10.1175/Jhm548.1.

[48] Liston, G.E.; Itkin, P.; Stroeve, J.; Tschudi, M.; Stewart, J.S.; Pedersen, S.H.; Reinking, A.K.; Elder, K. A Lagrangian Snow-Evolution System for Sea-Ice Applications (SnowModel-LG): Part I-Model Description. *J Geophys Res-Oceans* **2020**, 125, doi: 10.1029/2019JC015913.

[49] Liston, G.E. SnowModel (version 2020_10_02). **2020**, Retrieved from ftp://gliston.cira.colostate.edu/SnowModel/code/snowmodel_2020_10_02.zip.

[50] Liston, G.E.; Elder, K. A meteorological distribution system for high-resolution terrestrial modeling (MicroMet). *J Hydrometeorol* **2006**, 7, 217–234, doi: 10.1175/Jhm486.1.

[51] Liston, G.E. Local Advection of Momentum, Heat, and Moisture during the Melt of Patchy Snow Covers. *J Appl Meteorol* **1995**, 34, 1705–1715, doi:10.1175/1520-0450-34.7.1705.

[52] Liston, G.E.; Hall, D.K. An Energy-Balance Model of Lake-Ice Evolution. *J Glaciol* **1995**, 41, 373–382, doi:10.3189/S0022143000016245.

[53] Liston, G.E.; Haehnel, R.B.; Sturm, M.; Hiemstra, C.A.; Berezovskaya, S.; Tabler, R.D. Instruments and methods simulating complex snow distributions in windy environments using SnowTran-3D. *J Glaciol* **2007**, 53, 241-256, doi:10.3189/172756507782202865.

[54] Liston, G.E.; Sturm, M. A snow-transport model for complex terrain. *J Glaciol* **1998**, 44, 498-516, doi:10.3189/S0022143000002021.

[55] Liston, G.E.; Hiemstra, C.A. A Simple Data Assimilation System for Complex Snow Distributions (SnowAssim). *J Hydrometeorol* **2008**, 9, 989-1004, doi:10.1175/2008jhm871.1.

[56] Greene, E.M.; Liston, G.E.; Pielke, R.A. Simulation of above treeline snowdrift formation using a numerical snow-transport model. *Cold Reg Sci Technol* **1999**, 30, 135–144, doi:10.1016/S0165-232x(99)00008-7.

[57] Hiemstra, C.A.; Liston, G.E.; Reiners, W.A. Observing, modelling, and validating snow redistribution by wind in a Wyoming upper treeline landscape. *Ecol Model* **2006**, 197, 35-51, doi:10.1016/j.ecolmodel.2006.03.005.

[58] Sexstone, G.A.; Penn, C.A.; Liston, G.E.; Gleason, K.E.; Moeser, C.D.; Clow, D.W. Spatial Variability in Seasonal Snowpack Trends across the Rio Grande Headwaters (1984–2017). *J Hydrometeorol* **2020**, 21, 2713–2733, doi:10.1175/jhm-d-20-0077.1.

[59] Liston, G.E.; Polashenski, C.; Rösel, A.; Itkin, P.; King, J.; Merkouriadi, I.; Haapala, J. A Distributed Snow-Evolution Model for Sea-Ice Applications (SnowModel). *J Geophys Res-Oceans* **2018**, 123, 3786-3810, doi:10.1002/2017jc013706.

[60] Gesch, D.; Evans, G.; Oimoen, M.; Arundel, S. The national elevation dataset (pp. 83–110). *American society for photogrammetry and remote sensing*. **2018**. Retrieved from https://pubs.usgs.gov/publication/70201572.

[61] Homer, C.; Dewitz, J.; Yang, L.; Jin, S.; Danielson, P.; Xian, G.; Coulston, J.; Herold, N.; Wickham, J.; Megown, K. Completion of the 2011 National Land Cover Database for the conterminous United States–representing a decade of land cover change information. *Photogrammetric Engineering & Remote Sensing* **2015**, 81, 345-354.

[62] Salas, D., Stevens, J., Schulz, K. Rocky Mountain National Park, Colorado 2001-2005 Vegetation Classification and Mapping Project Report; Remote Sensing and GIS Group Technical Service Center Bureau of Reclamation: Denver, Colorado, **2005**. Retrieved from https://irma.nps.gov/DataStore/DownloadFile/425168.

[63] Xia, Y.; Mitchell, K.; Ek, M.; Sheffield, J.; Cosgrove, B.; Wood, E.; Luo, L.; Alonge, C.; Wei, H.; Meng, J. Continental-scale water and energy flux analysis and validation for the

North American Land Data Assimilation System project phase 2 (NLDAS-2): 1. Intercomparison and application of model products. *Journal of Geophysical Research: Atmospheres* **2012**, 117.

[64] Hall, D.K.; Riggs, G.A.; DiGirolamo, N.E.; Román, M.O. Evaluation of MODIS and VIIRS cloud-gap-filled snow-cover products for production of an Earth science data record. *Hydrol Earth Syst Sc* **2019**, 23, 5227–5241, doi:10.5194/hess-23-5227-2019.

[65] Koch, J.; Demirel, M.C.; Stisen, S. The SPAtial EFficiency metric (SPAEF): Multiple-component evaluation of spatial patterns for optimization of hydrological models. *Geoscientific Model Development* **2018**, 11, 1873–1886, https://doi.org/10.5194/gmd-11-1873-2018.

[66] McKay, M.D.; Beckman, R.J.; Conover, W.J. A comparison of three methods for selecting values of input variables in the analysis of output from a computer code. *Technometrics* **2000**, 42, 55–61.

[67] Falgout, J.T., Gordon J., Williams B., Davis, M.J. USGS Advanced Research Computing, USGS Denali Supercomputer: U.S. Geological Survey, **2024**, https://doi.org/10.5066/P9PSW367

[68] Gascoin, S.; Lhermitte, S.; Kinnard, C.; Bortels, K.; Liston, G.E. Wind effects on snow cover in Pascua-Lama, Dry Andes of Chile. *Advances in water resources* **2013**, 55, 25–39, https://doi.org/10.1016/j.advwatres.2012.11.013.

[69] Heldmyer, A.; Livneh, B.; Molotch, N.; Rajagopalan, B. Investigating the Relationship Between Peak Snow-Water Equivalent and Snow Timing Indices in the Western United States and Alaska. *Water Resour Res* **2021**, 57, e2020WR029395, doi:10.1029/2020WR029395.

[70] Selkowitz, D.J.; Forster, R.R. Automated mapping of persistent ice and snow cover across the western US with Landsat. *Isprs J Photogramm* **2016**, 117, 126–140, doi:10.1016/j.isprsjprs.2016.04.001.

[71] U.S. Geological Survey (USGS) Earth Resources Observation and Science (EROS) Center, Landsat Level-3 Fractional Snow Covered Area, Collection 2 [dataset], **2022**. https://doi.org/10.5066/P97ALZ2X.

[72] Dai, A. Temperature and pressure dependence of the rain-snow phase transition over land and ocean. *Geophysical Research Letters* **2008**, 35, L12802, doi:10.1029/2008gl033295.

[73] Wayand, N.E.; Marsh, C.B.; Shea, J.M.; Pomeroy, J.W. Globally scalable alpine snow metrics. *Remote Sensing of Environment* **2018**, 213, 61–72, doi:10.1016/j.rse.2018.05.012.

[74] Hammond, J.C.; Saavedra, F.A.; Kampf, S.K. How Does Snow Persistence Relate to Annual Streamflow in Mountain Watersheds of the Western U.S. With Wet Maritime and Dry Continental Climates? *Water Resour Res* **2018**, 54, 2605–2623, doi:10.1002/2017wr021899.

[75] Trujillo, E.; Molotch, N.P. Snowpack regimes of the Western United States. *Water Resour Res* **2014**, 50, 5611–5623, doi:10.1002/2013wr014753.

[76] Sturm, M.; Wagner, A.M. Using repeated patterns in snow distribution modeling: An Arctic example. *Water Resour Res* **2010**, 46, doi:10.1029/2010wr009434.

[77] Vögeli, C.; Lehning, M.; Wever, N.; Bavay, M. Scaling Precipitation Input to Spatially Distributed Hydrological Models by Measured Snow Distribution. *Frontiers in Earth Science* **2016**, 4, doi:10.3389/feart.2016.00108.

[78] Pflug, J.M.; Lundquist, J.D. Inferring Distributed Snow Depth by Leveraging Snow Pattern Repeatability: Investigation Using 47 Lidar Observations in the Tuolumne Watershed, Sierra Nevada, California. *Water Resour Res* **2020**, 56, e2020WR027243, doi:10.1029/2020wr027243.

[79] Deems, J.S.; Fassnacht, S.R.; Elder, K.J. Interannual Consistency in Fractal Snow Depth Patterns at Two Colorado Mountain Sites. *J Hydrometeorol* **2008**, 9, 977–988, doi:10.1175/2008jhm901.1.

[80] McGrath, D.; Sass, L.; O'Neel, S.; McNeil, C.; Candela, S.G.; Baker, E.H.; Marshall, H.-P. Interannual snow accumulation variability on glaciers derived from repeat, spatially extensive ground-penetrating radar surveys. *The Cryosphere* **2018**, 12, 3617–3633, doi:10.5194/tc-12-3617-2018.

[81] Arsenault, K.R.; Houser, P.R.; De Lannoy, G.J.M.; Dirmeyer, P.A. Impacts of snow cover fraction data assimilation on modeled energy and moisture budgets. *Journal of Geophysical Research: Atmospheres* **2013**, 118, 7489–7504, doi:10.1002/jgrd.50542.

[82] López-Moreno, J.I.; Gascoin, S.; Herrero, J.; Sproles, E.A.; Pons, M.; Alonso-González, E.; Hanich, L.; Boudhar, A.; Musselman, K.N.; Molotch, N.P.; et al. Different sensitivities of snowpacks to warming in Mediterranean climate mountain areas. *Environ Res Lett* **2017**, 12, 074006, doi:10.1088/1748-9326/aa70cb.

[83] Marshall, A.M.; Abatzoglou, J.T.; Link, T.E.; Tennant, C.J. Projected Changes in Interannual Variability of Peak Snowpack Amount and Timing in the Western United States. *Geophysical Research Letters* **2019**, 46, 8882–8892, doi:10.1029/2019gl083770.

[84] Musselman, K.N.; Lehner, F.; Ikeda, K.; Clark, M.P.; Prein, A.F.; Liu, C.; Barlage, M.; Rasmussen, R. Projected increases and shifts in rain-on-snow flood risk over western North America. *Nature Climate Change* **2018**, 8, 808–812, doi:10.1038/s41558-018-0236-4.

[85] Liston, G.E. Representing Subgrid Snow Cover Heterogeneities in Regional and Global Models. *Journal of Climate* **2004**, 17, 1381–1397, doi:10.1175/1520-0442(2004)017<1381:Rsschi>2.0.Co;2.

[86] López-Moreno, J.I.; Fassnacht, S.R.; Heath, J.T.; Musselman, K.N.; Revuelto, J.; Latron, J.; Morán-Tejeda, E.; Jonas, T. Small scale spatial variability of snow density and depth over complex alpine terrain: Implications for estimating snow water equivalent. *Advances in Water Resources* **2013**, 55, 40–52, doi:10.1016/j.advwatres.2012.08.010.

[87] Rittger, K.; Krock, M.; Kleiber, W.; Bair, E.H.; Brodzik, M.J.; Stephenson, T.R.; Rajagopalan, B.; Bormann, K.J.; Painter, T.H. Multi-sensor fusion using random forests for daily fractional snow cover at 30 m. *Remote Sensing of Environment* **2021**, 264, 112608, doi:10.1016/j.rse.2021.112608.

[88] Gascoin, S.; Barrou Dumont, Z.; Deschamps-Berger, C.; Marti, F.; Salgues, G.; López-Moreno, J.I.; Revuelto, J.; Michon, T.; Schattan, P.; Hagolle, O. Estimating Fractional Snow Cover in Open Terrain from Sentinel-2 Using the Normalized Difference Snow Index. *Remote Sens* **2020**, 12, 2904, https://doi.org/10.3390/rs12182904.

[89] Meyer, J.; Horel, J.; Kormos, P.; Hedrick, A.; Trujillo, E.; Skiles, S.M. Operational water forecast ability of the HRRR-iSnobal combination: an evaluation to adapt into production environments. *Geoscientific Model Development* **2023**, 16, 233–250, doi:10.5194/gmd-16-233-2023.

[90] Bair, E.H.; Rittger, K.; Davis, R.E.; Painter, T.H.; Dozier, J. Validating reconstruction of snow water equivalent in California's Sierra Nevada using measurements from the NASA Airborne Snow Observatory. *Water Resour Res* **2016**, 52, 8437–8460, doi:10.1002/2016wr018704.

[91] Dawson, N.; Broxton, P.; Zeng, X. Evaluation of Remotely Sensed Snow Water Equivalent and Snow Cover Extent over the Contiguous United States. *J Hydrometeorol* **2018**, 19, 1777–1791, doi:10.1175/jhm-d-18-0007.1.

[92] Broxton, P.D.; Dawson, N.; Zeng, X. Linking snowfall and snow accumulation to generate spatial maps of SWE and snow depth. *Earth and Space Science* **2016**, 3, 246–256, doi:10.1002/2016ea000174.

[93] Lehning, M.; Völksch, I.; Gustafsson, D.; Nguyen, T.A.; Stähli, M.; Zappa, M. ALPINE3D: a detailed model of mountain surface processes and its application to snow hydrology. *Hydrol Process* **2006**, 20, 2111–2128, doi:10.1002/hyp.6204.

[94] Pflug, J.M.; Hughes, M.; Lundquist, J.D. Downscaling Snow Deposition Using Historic Snow Depth Patterns: Diagnosing Limitations From Snowfall Biases, Winter Snow Losses, and Interannual Snow Pattern Repeatability. *Water Resour Res* **2021**, 57, e2021WR029999, doi:10.1029/2021wr029999.

[95] Reynolds, D.S.; Pflug, J.M.; Lundquist, J.D. Evaluating Wind Fields for Use in Basin-Scale Distributed Snow Models. *Water Resour Res* **2021**, 57, e2020WR028536, doi:10.1029/2020wr028536.

[96] Henn, B.; Newman, A.J.; Livneh, B.; Daly, C.; Lundquist, J.D. An assessment of differences in gridded precipitation datasets in complex terrain. *J Hydrol* **2018**, 556, 1205–1219, doi:10.1016/j.jhydrol.2017.03.008.

[97] Raleigh, M.S.; Small, E.E. Snowpack density modeling is the primary source of uncertainty when mapping basin-wide SWE with lidar. *Geophysical Research Letters* **2017**, 44, 3700–3709, doi:10.1002/2016gl071999.

[98] PlanetTeam. Planet Application Program Interface: In Space for Life on Earth. San Francisco, CA, **2024**. URL https://api.planet.com/ (accessed 3.1.24).

Disclaimer/Publisher's Note: The statements, opinions and data contained in all publications are solely those of the individual author(s) and contributor(s) and not of MDPI and/or the editor(s).

MDPI and/or the editor(s) disclaim responsibility for any injury to people or property resulting from any ideas, methods, instructions or products referred to in the content.

# Supplementary Material for: Fine Resolution Satellite Remote Sensing Improves Near Real-Time Spatially Distributed Snow Modeling

Graham A. Sexstone[1], Garrett A. Akie[1], David J. Selkowitz[2], Theodore B. Barnhart[2], David M. Rey[3], Claudia León-Salazar[4], Emily Carbone[5], Lindsay A. Bearup[6]

[1] U.S. Geological Survey, Colorado Water Science Center, Lakewood, CO, USA
[2] U.S. Geological Survey, Wyoming-Montana Water Science Center, Helena, MT, USA
[3] U.S. Geological Survey, Water Mission Area–Observing Systems Division, Hydrologic Remote Sensing Branch, Lakewood, CO, USA
[4] U.S. Bureau of Reclamation, Eastern Colorado Area Office, Loveland, CO, USA
[5] Northern Colorado Water Conservancy District, Berthoud, CO, USA
[6] U.S. Bureau of Reclamation, Technical Service Center, Lakewood, CO, USA

Disclaimer
Any use of trade, firm, or product names is for descriptive purposes only and does not imply endorsement by the U.S. Government.

## Supporting Information S1

To develop the land cover classification used within SnowModel for this study, we utilized the National Park Service (NPS) Vegetation Mapping Inventory Project dataset for Rocky Mountain National Park (RMNP) described in Salas (2005). This dataset was selected because it provides the detailed representation of tundra vegetation classes required for accurately modeling blowing snow dynamics in alpine areas, which experience extensive redistribution of snow cover by wind (Liston et al. 2007). We crosswalked the 46 land cover/vegetation classes represented in the NPS vegetation inventory to 13 simplified vegetation/land cover classes defined for use with SnowModel (Liston and Elder 2006). In order to classify the entire model domain, including areas outside the extent of the NPS dataset, we constructed a cloud-free 3-meter (m) resolution multispectral imagery composite using data acquired by PlanetScope satellites August 11–13, 2018 (PlanetTeam 2024). We used the crosswalked NPS vegetation classification to train a random forest model to identify the 13 land cover classes using the PlanetScope image composite along with topographic layers derived from the digital elevation model (DEM) (Akie et al. 2025). The random forest classification model was then applied to produce a 3 m land cover classification raster covering parts of the model domain not included in the NPS classification, which was then mosaicked together with the crosswalked NPS vegetation classification, resulting in a 3 m raster land cover classification covering the full model domain. The 3 m raster land cover classification was then regridded using majority resampling to match the 30 m resolution of the model grid (Akie et al. 2025).

Supporting Information S2

To compute the mean annual snow persistence (SP), we acquired all U.S. Geological Survey (USGS) Landsat Level 3 Fractional Snow Covered Area (USGS 2022) tiles covering the model

domain where the Landsat scene used to produce the tile was acquired between January 1 and July 31 for calendar years 2000–2020. All tiles available for a single date were mosaicked together and regridded to match the extent and grid of the SnowModel domain. For each individual month (January–July), we computed 2 grids covering the model domain: (1) total count (per 30-m grid cell) of cloud-free observations, and (2) count (per 30-m grid cell) of cloud-free observations where snow-cover fraction > 0. The pixelwise ratio of cloud-free, snow-cover instances to total cloud-free instances was then computed for each pixel. This ratio was then multiplied by the number of days in the month, resulting in a mean snow cover days count for each of the seven months. The total mean snow cover days for the January–July period was then computed by summing the mean snow cover days by month.

**Table A-S1.—SNOTEL stations (NRCS 2024) used for the study and their performance statistics (root mean squared error [RMSE], mean absolute error [MAE], Pearson's correlation [R], Nash–Sutcliffe efficiency [NSE]) based on all SnowModel runs including (a) default SnowModel version without SNOTEL assimilation (SnowModeldefault_noassim), (b) default SnowModel version (SnowModeldefault), (c) calibrated SnowModel version (SnowModelcalibrated), and (d) calibrated with Landsat correction field SnowModel version (SnowModelLandsat) (Akie et al. 2025)**

| Model Version | SNOTEL Station | SWE RMSE, m | SWE MAE, m | SWE Pearson's R | SWE NSE | Density RMSE, kg/m3 | Density MAE, kg/m3 | Density Pearson's R | Density NSE |
|---|---|---|---|---|---|---|---|---|---|
| SnowModeldefault_noassim | Lake Irene | 0.23 | 0.19 | 0.89 | -0.02 | 93.78 | 77.86 | 0.73 | -1.04 |
| SnowModeldefault | Lake Irene | 0.16 | 0.13 | 0.96 | 0.50 | 104.75 | 92.12 | 0.73 | -1.47 |
| SnowModelcalibrated | Lake Irene | 0.17 | 0.14 | 0.95 | 0.42 | 82.99 | 58.27 | 0.75 | -0.57 |
| SnowModelLandsat | Lake Irene | 0.12 | 0.10 | 0.93 | 0.72 | 80.22 | 52.62 | 0.75 | -0.44 |
| SnowModeldefault_noassim | Never Summer | 0.25 | 0.20 | 0.78 | -0.42 | 80.22 | 61.60 | 0.74 | -0.30 |
| SnowModeldefault | Never Summer | 0.18 | 0.15 | 0.91 | 0.28 | 87.09 | 73.13 | 0.78 | -0.37 |
| SnowModelcalibrated | Never Summer | 0.19 | 0.16 | 0.88 | 0.17 | 78.73 | 60.91 | 0.81 | -0.17 |
| SnowModelLandsat | Never Summer | 0.14 | 0.11 | 0.93 | 0.60 | 68.74 | 50.73 | 0.83 | 0.18 |
| SnowModeldefault_noassim | Phantom Valley | 0.11 | 0.08 | 0.67 | -0.29 | 123.52 | 103.08 | 0.44 | -2.83 |
| SnowModeldefault | Phantom Valley | 0.07 | 0.05 | 0.90 | 0.52 | 123.94 | 107.33 | 0.56 | -2.61 |
| SnowModelcalibrated | Phantom Valley | 0.07 | 0.05 | 0.89 | 0.51 | 103.03 | 75.62 | 0.70 | -1.71 |
| SnowModelLandsat | Phantom Valley | 0.04 | 0.03 | 0.94 | 0.79 | 101.17 | 73.23 | 0.69 | -1.30 |
| SnowModeldefault_noassim | Willow Creek Pass | 0.16 | 0.12 | 0.64 | -0.40 | 121.40 | 97.33 | 0.53 | -5.86 |
| SnowModeldefault | Willow Creek Pass | 0.11 | 0.09 | 0.87 | 0.30 | 128.01 | 109.32 | 0.62 | -5.30 |
| SnowModelcalibrated | Willow Creek Pass | 0.14 | 0.11 | 0.73 | -0.07 | 106.47 | 74.52 | 0.64 | -4.05 |
| SnowModelLandsat | Willow Creek Pass | 0.06 | 0.04 | 0.94 | 0.83 | 103.28 | 71.63 | 0.70 | -2.88 |
| SnowModeldefault_noassim | Willow Park | 0.17 | 0.13 | 0.85 | 0.09 | 97.06 | 77.22 | 0.51 | -1.12 |
| SnowModeldefault | Willow Park | 0.11 | 0.08 | 0.96 | 0.65 | 101.47 | 84.07 | 0.55 | -1.29 |
| SnowModelcalibrated | Willow Park | 0.11 | 0.09 | 0.95 | 0.59 | 97.05 | 72.78 | 0.61 | -1.09 |
| SnowModelLandsat | Willow Park | 0.06 | 0.04 | 0.94 | 0.88 | 92.00 | 63.64 | 0.57 | -0.86 |

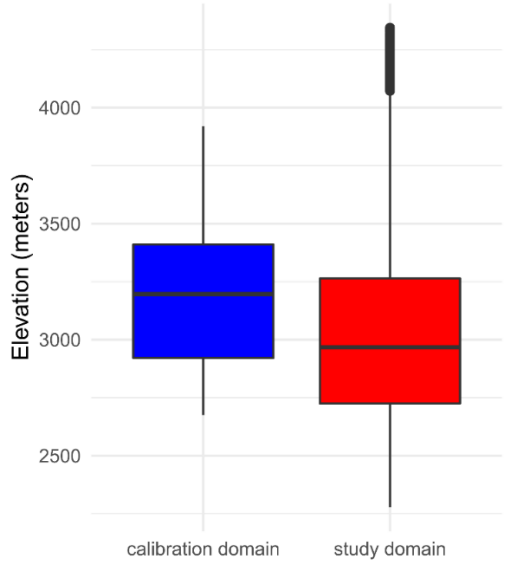


**Figure A-S1.—Boxplot comparison between calibration domain elevation distribution and entire study domain elevation distribution (Akie et al. 2025).**

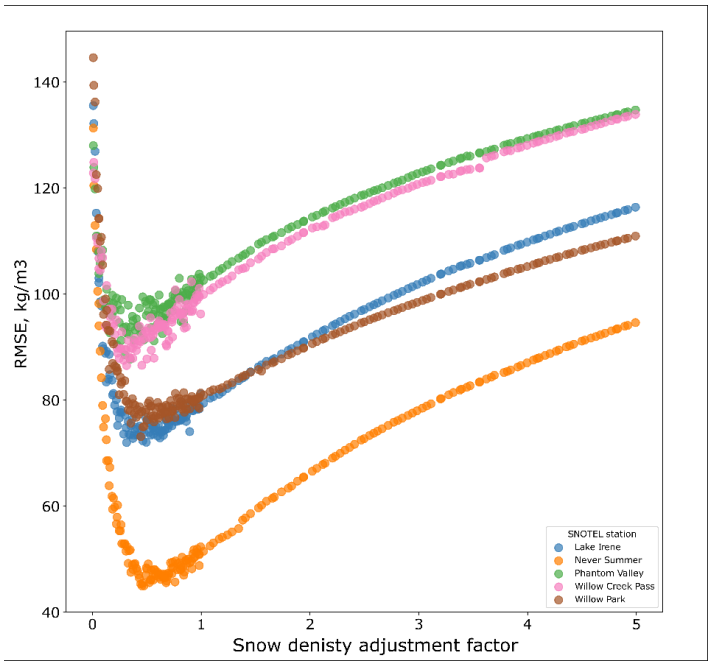


**Figure A-S2.—Root mean squared error (RMSE) between simulated SnowModelcalibrated and observed SNOTEL snow density (NRCS 2024) across a range of snow density adjustment factor parameter values highlighting the calibration converging on a value of 0.4 (Akie et al. 2025).**

**Table A-S2.—Performance statistics computed across the study domain between simulated SnowModel snow persistence (SP) and snow-covered area (SCA) and observed Landsat SP (USGS 2022) and MODIS SCA (Hall et al. 2019) time series, respectively. Performance statistics calculated using the spatial efficiency metric (SPAEF) (including correlation [α], ratio of coefficient of variation [β], and histogram match [γ]) (Koch et al. 2018) as well as the root mean squared error (RMSE) for the default SnowModel version, calibrated SnowModel version, and calibrated with Landsat correction field SnowModel version (Akie et al. 2025)**

| SnowModel version | Landsat Mean Annual SP SPAEF | Landsat Mean Annual SP Alpha | Landsat Mean Annual SP Beta | Landsat Mean Annual SP Gamma | MODIS Daily SCA RMSE (percent) |
|---|---|---|---|---|---|
| SnowModeldefault | 0.10 | 0.75 | 1.05 | 0.13 | 13.3 |
| SnowModelcalibrated | 0.22 | 0.77 | 1.00 | 0.26 | 11.3 |
| SnowModelLandsat | 0.10 | 0.95 | 1.19 | 0.12 | 11.1 |

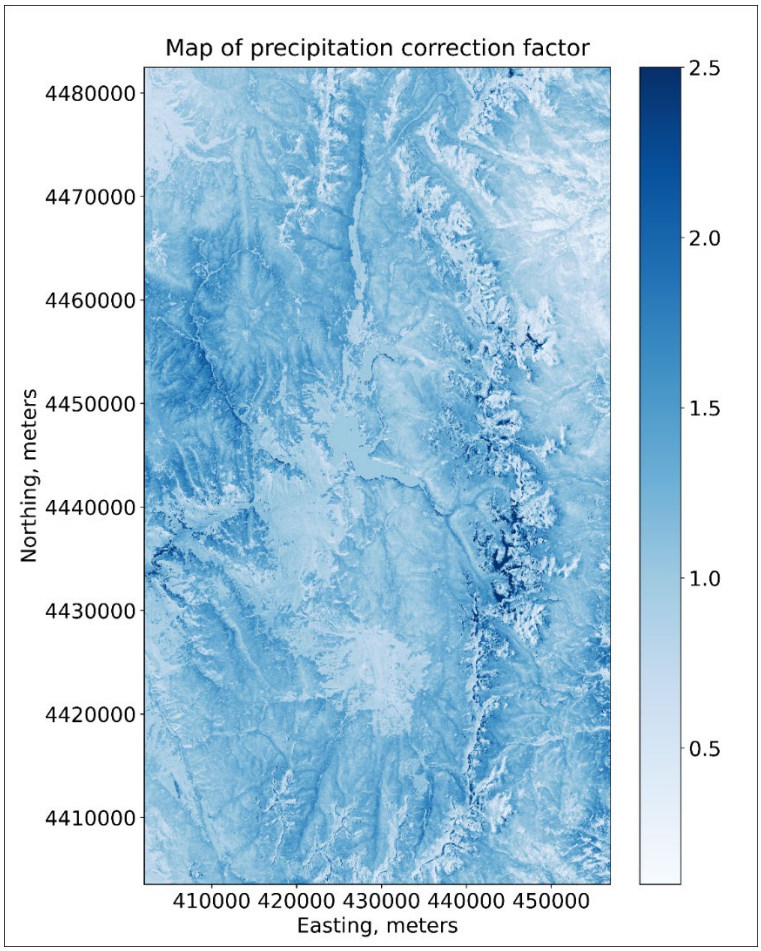


**Figure A-S3.—Map of precipitation bias correction field developed for the study area (Akie et al. 2025).**

| | | April 18, 2022 | | | | | May 26, 2022 | | | | |
|---|---|---|---|---|---|---|---|---|---|---|---|
| | Model version | SNODAS | SnowModel default_noassim | SnowModel defult | SnowModel calibrated | SnowModel Landsat | SNODAS | SnowModel default_noassim | SnowModel$_d$ efult | SnowModel calibrated | SnowModel Landsat |
| ALL ELEVATIONS | Model mean SWE (mm) | 272 | 85 | 292 | 245 | 196 | 138 | 54 | 190 | 134 | 98 |
| | ASO mean SWE (mm) | 223 | 223 | 223 | 223 | 223 | 104 | 104 | 104 | 104 | 104 |
| | Mean Error (mm) | 48 | -139 | 69 | 22 | -28 | 34 | -50 | 86 | 31 | -6 |
| | Mean Absolute Error (mm) | 139 | 159 | 144 | 122 | 87 | 105 | 82 | 110 | 74 | 54 |
| | Root Mean Squared Error (mm) | 193 | 219 | 204 | 173 | 137 | 199 | 172 | 216 | 162 | 121 |
| | Percent Bias (%) | 21.6 | -62.0 | 30.7 | 9.8 | -12.5 | 32.8 | -48.0 | 83.5 | 29.6 | -5.4 |
| | Nash-Sutcliffe Efficiency | 0.13 | -0.13 | 0.02 | 0.30 | 0.56 | 0.00 | 0.25 | -0.18 | 0.33 | 0.63 |
| | Pearson correlation coefficient | 0.55 | 0.58 | 0.52 | 0.60 | 0.77 | 0.47 | 0.56 | 0.68 | 0.72 | 0.81 |
| HIGH ELEVATIONS | Model mean SWE (mm) | 405 | 183 | 456 | 362 | 320 | 309 | 150 | 493 | 362 | 273 |
| | ASO mean SWE (mm) | 406 | 406 | 406 | 406 | 406 | 284 | 284 | 284 | 284 | 284 |
| | Mean Error (mm) | -1 | -223 | 50 | -44 | -86 | 25 | -134 | 210 | 78 | -11 |
| | Mean Absolute Error (mm) | 188 | 277 | 203 | 165 | 137 | 221 | 218 | 272 | 191 | 135 |
| | Root Mean Squared Error (mm) | 260 | 327 | 290 | 235 | 200 | 307 | 292 | 363 | 273 | 203 |
| | Percent Bias (%) | -0.2 | -55.0 | 12.2 | -10.9 | -21.1 | 8.8 | -47.1 | 73.9 | 27.6 | -3.8 |
| | Nash-Sutcliffe Efficiency | -0.38 | -1.18 | -0.72 | -0.13 | 0.18 | -0.42 | -0.29 | -0.99 | -0.13 | 0.38 |
| | Pearson correlation coefficient | 0.04 | 0.05 | 0.03 | 0.38 | 0.63 | 0.01 | 0.29 | 0.35 | 0.48 | 0.69 |
| MIDDLE ELEVATIONS | Model mean SWE (mm) | 209 | 37 | 213 | 191 | 136 | 54 | 6 | 40 | 21 | 11 |
| | ASO mean SWE (mm) | 135 | 135 | 135 | 135 | 135 | 14 | 14 | 14 | 14 | 14 |
| | Mean Error (mm) | 74 | -98 | 78 | 56 | 1 | 39 | -8 | 26 | 7 | -3 |
| | Mean Absolute Error (mm) | 117 | 102 | 116 | 101 | 64 | 47 | 14 | 30 | 17 | 13 |
| | Root Mean Squared Error (mm) | 150 | 139 | 143 | 133 | 91 | 114 | 44 | 65 | 50 | 38 |
| | Percent Bias (%) | 54.9 | -72.5 | 58.0 | 41.2 | 0.8 | 275.2 | -57.7 | 179.9 | 50.5 | -22.0 |
| | Nash-Sutcliffe Efficiency | -0.56 | -0.32 | -0.41 | -0.22 | 0.44 | -4.65 | 0.15 | -0.86 | -0.10 | 0.38 |
| | Pearson correlation coefficient | 0.63 | 0.62 | 0.44 | 0.49 | 0.71 | 0.49 | 0.49 | 0.65 | 0.62 | 0.63 |
| LOW ELEVATIONS | Model mean SWE (mm) | 18 | 0 | 76 | 23 | 1 | 0 | 0 | 0 | 0 | 0 |
| | ASO mean SWE (mm) | 10 | 10 | 10 | 10 | 10 | 0 | 0 | 0 | 0 | 0 |
| | Mean Error (mm) | 8 | -10 | 66 | 13 | -9 | --- | --- | --- | --- | --- |
| | Mean Absolute Error (mm) | 15 | 10 | 72 | 27 | 10 | --- | --- | --- | --- | --- |
| | Root Mean Squared Error (mm) | 20 | 22 | 95 | 48 | 23 | --- | --- | --- | --- | --- |
| | Percent Bias (%) | 81.6 | -99.7 | 664.4 | 126.7 | -91.2 | --- | --- | --- | --- | --- |
| | Nash-Sutcliffe Efficiency | -0.07 | -0.25 | -22.50 | -4.92 | -0.36 | --- | --- | --- | --- | --- |
| | Pearson correlation coefficient | 0.44 | 0.09 | -0.04 | 0.00 | 0.19 | --- | --- | --- | --- | --- |

Figure A-S4.—Performance statistics based on grid-by-grid SNODAS, SnowModel [default SnowModel version without SNOTEL assimilation (SnowModeldefault_noassim), default SnowModel version (SnowModeldefault), calibrated SnowModel version (SnowModelcalibrated), and calibrated with Landsat correction field SnowModel version (SnowModelLandsat)] simulated snow water equivalent (SWE) (Akie et al. 2025) compared to Airborne Snow Observatories (ASO)-derived SWE for the 18 April 2022 and 26 May 2022 across the Windy Gap Basin (ASO 2024). Performance statistics are provided for all elevations, high elevations (>3,124 m), middle elevations (2,438 – 3,124 m), and low elevations (<2,438 m). "---" indicates zero snow observed.

# References

Akie, G.A.; Barnhart, T.B.; Selkowitz, D.; Sexstone, G.A. Historical simulated snowpack for the Willow Creek and Big Thompson, CO watersheds and vicinity, water years 1994-2023. U.S. Geological Survey Data Release 2025, https://doi.org/10.5066/P9NTGM51.

ASO. Airborne Snow Observatories (ASO). 2024, URL https://data.airbornesnowobservatories.com/ (accessed 3.1.24).

Hall, D.K.; Riggs, G.A.; DiGirolamo, N.E.; Román, M.O. Evaluation of MODIS and VIIRS cloud-gap-filled snow-cover products for production of an Earth science data record. Hydrol Earth Syst Sc 2019, 23, 5227-5241, doi:10.5194/hess-23-5227-2019.

Koch, J.; Demirel, M.C.; Stisen, S. The SPAtial EFficiency metric (SPAEF): Multiple-component evaluation of spatial patterns for optimization of hydrological models. Geoscientific Model Development 2018, 11, 1873–1886, https://doi.org/10.5194/gmd-11-1873-2018.

Liston, G.E.; Elder, K. A distributed snow-evolution modeling system (SnowModel). J Hydrometeorol 2006, 7, 1259–1276, doi:10.1175/Jhm548.1.

Liston, G.E.; Haehnel, R.B.; Sturm, M.; Hiemstra, C.A.; Berezovskaya, S.; Tabler, R.D. Instruments and methods simulating complex snow distributions in windy environments using SnowTran-3D. J Glaciol 2007, 53, 241–256, doi:10.3189/172756507782202865.

NRCS. Natural Resources Conservation Service (NRCS) Snow and Water Interactive Map. 2024, URL https://www.nrcs.usda.gov/resources/data-and-reports/snow-and-water-interactive-map (accessed 3.1.24).

PlanetTeam. Planet Application Program Interface: In Space for Life on Earth. San Francisco, CA, 2024. URL https://api.planet.com/ (accessed 3.1.24).

Salas, D., Stevens, J., Schulz, K. Rocky Mountain National Park, Colorado 2001–2005 Vegetation Classification and Mapping Project Report; Remote Sensing and GIS Group Technical Service Center Bureau of Reclamation: Denver, Colorado, 2005. Retrieved from https://irma.nps.gov/DataStore/DownloadFile/425168.

U.S. Geological Survey (USGS) Earth Resources Observation and Science (EROS) Center, Landsat Level-3 Fractional Snow Covered Area, Collection 2 [dataset], 2022. https://doi.org/10.5066/P97ALZ2X.